Summer 2024

Optimizing the Total Life Cycle of Li-Ion Batteries: from Constant Gradient Charging to Aged Cell Performance Restoration

Kasim Adesegun Adewuyi
Missouri University of Science and Technology

OPTIMIZING THE TOTAL LIFE CYCLE OF LI-ION BATTERIES: FROM CONSTANT GRADIENT CHARGING TO AGED CELL PERFORMANCE RESTORATION

by

KASIM ADESEGUN ADEWUYI

A DISSERTATION

Presented to the Graduate Faculty of the

MISSOURI UNIVERSITY OF SCIENCE AND TECHNOLOGY

In Partial Fulfillment of the Requirements for the Degree

DOCTOR OF PHILOSOPHY

in

MECHANICAL ENGINEERING

2024

Approved by:

Jonghyun Park, Advisor
Anthony Okafor
Frank Liou
Jonathan Kimball
Douglas Bristow

PUBLICATION DISSERTATION OPTION

This dissertation consists of the following two articles, formatted in the style used by the Missouri University of Science and Technology:

Paper I, found on pages 10–44, is intended for submission to *Journal of Power Sources*.

Paper II, found on pages 45–95, is intended for submission to *Journal of Applied Energy*.

ABSTRACT

As demand for Lithium-Ion Batteries (LIBs) have skyrocketed over the past decade, the need for better charging methodologies and recycling methods have become vitally important. At a fundamental level, this dissertation strives to fulfill the green promise of a future without fossil fuels. In order to promote a transition away from fossil fuels, LIBs for vehicles require ultrafast charging times equivalent to a normal vehicle (6 mins). However, this process leads to high volume expansion for next generation electrode materials which causes degradation. Without limiting this factor, the environmental impact shifts from oil rigs to Li mines and landfills.

The first paper shows a novel optimal charging protocol focusing on the relationship between concentration gradients and degradation, and state-of-charge-dependent diffusivity. The paper demonstrates a constant gradient constant voltage charging approach (CGCV) that controls this gradient in combination with diffusivity can create novel charging current profiles that maintain sufficiently low maximum stress.

The second paper presents a facile direct recycling remanufacturing process that does not rely on elevated temperatures or harsh chemicals to recover pristine metals (Li, Ni, Co, etc) from spent electrodes. This paper introduces a more minimally invasive approach. A detailed investigation of treatment steps including plasma treatment, drying methodology, pressing, type of slurry addition, has enabled the development of an optimized process achieving high cell viability (>80%) and capacity performance for highly degraded electrodes.

ACKNOWLEDGMENTS

Firstly, I want to convey my deepest appreciation to my advisor, Dr. Jonghyun Park, for giving me the opportunity to pursue a Ph.D. He provided critical aid and direction throughout my time at MST. Beyond that he also provided some great life advice with some very poetic anecdotes and metaphors. His aid, candor and expertise have been instrumental in all that I have achieved over this long journey, and it would have been impossible without them. Naturally, I am also extremely grateful for the financial support along the way, especially the GAANN Fellowship and NSF funding.

Secondly, I want to give my warmest regards to all my committee members, Dr. Anthony Okafor, Dr. Frank Liou, Dr. Jonathan Kimball and Dr. Douglas Bristow. I am forever grateful to these distinguished scholars for agreeing to serve on my committee. Additionally, I would like to extend my warmest regards to Dr. Okafor who was a valuable sounding board and a font of wisdom as I navigated some grim times here. Finally, I would like to thank my colleagues who have already departed MST: Nima Lofti, Jie Li, Brody Reimann, Hiep Pham and Tazdik Patawary Plateau. As well as my colleagues that will follow me: Kiernan O'Boyle, Jacob Sutton, Emmanuel Olugbade. All of them were immensely helpful on this journey and I hope I returned the favor in equal measure.

Lastly, I want to thank my father and mother for not just their financial support and advice when things were difficult. They were always there to pick me up and provide extra motivation in the darkest hours and thus I am eternally grateful for their love and support on this long and winding journey called life. May we all, "Live Long and Prosper".

TABLE OF CONTENTS

LIST OF ILLUSTRATIONS

PAPER I Page

PAPER II

LIST OF TABLES

NOMENCLATURE

Symbol	Description
CCCV	Constant Current Constant Voltage
CGCV	Constant Gradient Constant Voltage
CC	Constant Current
CG	Constant Gradient
SOC	State of Charge
LIBs	Lithium-ion Batteries
EVs	Electric Vehicles
LMO	Lithium Manganese Oxide (Li_2MnO_4)
NMC	Lithium Nickel Manganese Cobalt
MCMB	MesoCarbon Microbeads Graphite
MS	Multistep Constant Current
MCC	Multistage Constant Current
CP	Constant Power
CB	Carbon Black
PVDF	Polyvinylidene Fluoride
NMP	N-Methlyl-2-pyrrolidiene
PE/PP	Propylene/Polyester
DMC	Dimethyl Carbonate
LiTFSi	Lithium bis(trifluromethanesulfonly)imide
CP-##	NMC Cathodes treated with plasma treatment and pressing

CN-##	NMC cathodes treated with plasma treatment but no pressing
CW-##	NMC cathodes treated with pressing but no plasma treatment
CU-##	NMC cathodes treated with unsalted (normal) slurry
CS-##	NMC cathodes treated with salted slurry
A1-##	MCMB anodes treated with pressing and plasma treatment
HP-##	NMC cathodes dried on hot plate
VO-##	NMC cathodes dried in vacuum oven
FA-##	MCMB anodes fused with cathodes of the corresponding number
FC-##	NMC cathodes fused with anodes of the corresponding number
Cap	Capacity (mAh/g)
NSSE	Normalized Square of Errors
GITT	Galvanostatic Intermittent Titration Technique
OCV, U	Open Circuit Voltage (V)
lp	Cathode thickness (um)
Rp	Particle radius of cathode (um)
kp	Reaction rate coefficient for cathode ($m^{2.5}mol^{-0.5}s$)
Dp, D	Diffusivity of the cathode (m^2/s)
Cs,max	Maximum solid phase concentration of the cathode (mol/m^3)
Ce	Electrolyte concentration (mol/m^3)
C	Concentration (mol/m^3)
ε,ep	Electrolyte phase volume fraction
ε,sp	Solid phase volume fraction
Rcell	Cell Resistance (Ω)

dt	Time step (s)
τ	Current pulse length (s)
Vm	Molar volume (mol/m^3)
n_m	Number of moles in the electrode (mol)
S	Electrode surface area (m^2)
ΔEs	Voltage change during current pulse (V)
ΔEt	Voltage change from last rest to current rest (V)
G	Concentration gradient at the surface (mol/m^4)
i	Current (mA)
σ	Surface stress (Pa)
ϕ1,p	Solid phase potential of cathode (V)
q	Average solid phase flux
j	Molar flux density

1. INTRODUCTION

1.1. BACKGROUND AND RESEARCH OBJECTIVES

The United Nations Intergovernmental Panel on Climate Change (IPCC) states that to advert catastrophic climate change, the global temperature must hold to 2°C. Crossing this red line will result in water shortages, widespread famines, more extreme weather, disease proliferation which will trigger mass migration events from climate refugees as some regions of the globe become unlivable. Additionally, it could trigger resource wars over the dwindling supply of critical resources. To prevent these apocalyptic scenarios, humanity must end its dependance on fossil fuels and hastily transition towards a green future dominated by renewable solutions. However, critical renewable options such as solar energy and wind turbines are intermittent energy sources that require storage to align supply with demand. Furthermore, according to the US Department of Energy, the transportation sector accounts 30% of total US energy consumption and 70% of all American petroleum consumption.

Thus, Lithium-Ion Batteries (LIBs) have emerged as key solution to these problems with their combination of high energy and power with large capacity. Additionally, they provide extreme versatility in usage ranging from small portable electronics to Electric Vehicles (EVs) and storage systems for large solar arrays. By 2030, the total demand for LIBs is estimated to pass 2800 GWh with the total number of Electric Vehicles (EVs) reaching 50 million, which is 6.5 times the number at the start of the decade [1]. However, their wide scale adoption is hampered by three factors. First, the availability of critical elements like lithium and cobalt for their construction. Second, environmental and health

concerns stemming from the mining of critical elements and their disposal. Third, EVs specifically lag far behind the 6 minute average fueling time of traditional automobiles [2].

The explosive growth in demand for LIBs is already taxing the global supply of vital metals, especially lithium, cobalt, and nickel. Lithium supply is already struggling to meet demand as of 2023 with Co expected to join it as early as 2024. Furthermore, the International Energy Agency predicts that by as early as 2028, lithium demand will exceed supply by 2 to 1 [2]. Negative externalities caused by wars, pandemics or geopolitical priorities could constrict the global supply chain. Over 50% of proven cobalt reserves are concentrated in the Democratic Republic of the Congo while most of the world's lithium supply is concentrated in Chile, Argentina, and Bolivia.

The environmental concerns and health risks from mining are numerous but a general overview of the most significant is provided. In South America, lithium carbonate is produced by evaporating salt lakes in shallow ponds. These ponds are prone to flooding which can devastate farmland and local wildlife that depends on nearby rivers. Any loss in wildlife could result in cyanobacteria blooms which produce dangerous microcystin toxins known to cause liver failure in vertebrates[3]. Additionally, the PVC barriers for these basins are susceptible to chemical reactions resulting in compounds especially hazardous to reproductive health. For disposal, toxic fluorine from electrolytes and heavy metals like cobalt can seep into the groundwater supply from landfills. Incineration can worsen the issues transforming the heavy metals, fluorine and organic materials into toxic dust clouds. Fortunately, recycling could meet 30-40% of domestic Li and Co demand by 2035 if current adoption of EVs persists. This would alleviate both supply and the environmental/health concerns showing why recycling is critical to a green future.

Wide scale adoption of EVs is limited by fast charging while fast charging is in turn limited by degradation. The three forms of degradation are thermal, Li plating and mechanical. During fast charging, thermal degradation is caused by irreversible heat generation which has a quadratic relationship with current. The US National Renewable Energy Laboratory has found that reducing temperature from 35^{o}C to 20^{o}C doubles cell life [4]. Fortunately, proper thermal management using air or liquid cooling systems can mitigate these issues. Lithium plating stems from side reactions between Li-ions and the electrolyte causing dendrites to grow on the electrode surface. These dendrites cause capacity losses as Li is removed from circulation and can eventually short circuit cells by growing through the separator. Mechanical degradation is the result of concentration gradient as fast charging does not allow sufficient time for Li-ions to properly intercalate into the electrode. This buildup increases surface stress until a critical fracture point is reached which is alleviated through crack propagation [5]. These fractures expand the surface area of the electrode allowing for more Li-ions to intercalate. Models can be generated to create shock maps for different C-rates and electrode particle size, but these models are difficult to validate. This is due to the complexity of real boundary conditions and the difficulty in measuring initial crack length and critical fracture points.

This work seeks to create a facile recycling process for spent electrodes that will help address supply shortfalls while limiting the environmental and health impacts caused by mining and disposal. Additionally, a novel charging algorithm is presented that manages the concentration gradient to limit crack propagation. Since the real critical fracture point is difficult to determine experimentally, it is designed to maintain surface stress below a maximum stress defined by the CCCV charging profile.

1.2. OPTIMAL CHARGING

The common goal of all optimal charging approaches is to maximize charging rate and minimize degradation. To this end, the three primary approaches to boosting performance are materials engineering at the cell level, battery management systems via pack design, and novel charging algorithms.

Cell design is the broadest category that encompasses Li-ion diffusion control, surface modification, nanostructuring, dopant manipulation, surface modification and composite hybrid design solutions. Diffusion control techniques increase diffusivity by lowering activation energy [2]. For instance, $LiNiMnO_2$ has a high activation energy because Oxygen atoms create larger gaps leading to disorder in the Li-Ni sites. Thus, synthesizing $LiNiMnO_2$ with less interlayer disorder can reduce activation energy by about 40% which doubles energy density and reduces capacity fade by 25% [6]. Surface modification uses coatings to stabilize SEI layers reducing degradation while also boosting electrical or ionic conductivity. A simple carbon coating on spinel $LiMn_2O_4$ nanoparticles greatly enhances performance allowing 47% capacity retention even at extremely high currents of 300C [2]. Coatings need not be so simple as cheaper low ionic conductivity materials like Lithium-titanate can be coated with high ionic conductivity rutile. This boosts capacity to 110 mAh/g at 11C which is an order of magnitude increases relative to the uncoated version [2]. Nanostructuring increases diffusivity by maximizing surface area and shortening the solid-state diffusion lengths. This leads to the creation of various shapes including 2D sheets, nanotubes, and hollow structures. These novel structures characterized by high surface area allow for more positions for interfacial reactions of Li-ions across the electrode/electrolyte interface. In constant, dopant manipulation enhances

conductivity by introducing new elements to create excess and deficiency of electrons in the bulk material. This provides more pathways for Li-ions to intercalate into electrode. Graphene anodes can use either Boron or Nitrogen doping to achieve high capacity (> 200 mAh/g) full charging in only 30 seconds [7]. Composite hybrid solutions go beyond mere coating and introduce conductive additives (carbon, polymer or metallic compounds) to enhance ionic and electrical conductivity. For example, a Si-C composite with a hierarchical structure outperforms annealed carbon black by 870 mAh/g to 40 mAh/g at 8C because Si opens new pathways for Li-ions to rapidly disperse through [8].

Secondly, battery management systems regulate charge voltage and current to extend battery life and charging efficiency. They accomplish this by minimizing the constant voltage regime in favor of the more efficient constant current regime. Traditional analog controllers have given way to newer digital controllers because analog systems rely on capacitors and resistors which are susceptible to environmental conditions. Digital controllers allow for easier system manufacturing and maintenance along with real time environmental adaptation, robustness against noise, and programmable compensators for complicated control methods [9].

Finally, alternative charging methodologies are any charging profiles that deviate from the standard CCCV. These solutions include multistage charging (ascending/descending constant current steps), pulse charging (repeated long high current charge steps with short low current discharge and/or rest steps) and varying current methods (continuously updates current with respect to some parameter) [10]. Here battery characteristics like internal resistance, impedance evolution, and temperature changes among other factors are used to develop optimal charging methodologies. Thus, leading to

high variation in approach depending on which parameters are selected and battery chemistry.

This dissertation focuses on charging-based methodologies because they are independent of cell architecture and battery system design allowing for universal application. The novel approach presented here seeks to regulate degradation using an optimal charging methodology that adjusts current with respect to concentration gradient using diffusivity which varies based on the state of charge (SOC). This novel constant gradient technique allows for a significant reduction in charging time while degradation is controlled by limiting crack propagation.

1.3. REMANUFACTURING

Remanufacturing has become of vital importance due to a confluence of events including skyrocket demand for critical metals (Li, Ni, Co) , environmental degradation caused by mining operations primarily groundwater contamination and battery disposal causing health concerns linked to particulate matter release when batteries are disposed of via incineration, along with further water contamination [11]. This is not even accounting for supply chain issues caused by Covid-19 and future pandemics or geopolitical tensions as critical metals are not evenly distributed [12]. Recycling via remanufacturing processes can address all these issues, however these processes have environmental impact, water usage and energy usage concerns that must be considered.

Pyrometallurgy (physical), hydrometallurgy and direct recycling are the three classifications of remanufacturing. Pyrometallurgy is the primary industrial method characterized by broad applicability for various battery chemistries, simplicity, and ease of

scalability. The key components of this process are roasting, smelting, refining and extraction. Batteries are smelted in furnaces at high temperatures (> 500^{o}C) using basic oxidation and reduction reactions to recover a valuable mixed metal alloy (Cu, Co, Ni, Fe, etc.). However, these high temperatures result in toxic gases, mixed slag which is potentially hazardous, and high energy consumption. These negative impacts can be lessened by modifying the roasting process using chemical reagents (chlorides, sulfates, nitrides) and/or reducing gases which also serve to enhance the Li extraction rate from the mixed slag [1]. The most optimized processes can reach recovery rates of 90% for Li, Co, Mn and Ni with typical approaches being far lower [13].

Hydrometallurgy offers extreme flexibility and the ability to extract the valuable pure metals through a precise mastery liquid phase chemical reaction. Leaching and separation are the primary steps of this process with leaching determining recovery rate and procedure cost. This reliance on acid leaching and solvent extraction techniques produces substantial amounts of wastewater. What this process lacks in scalability is made up for by the high purity of its recovered metals typically reaching >95% with the best processes >99% for Li, Ni, Co [14]. Additionally, the specificity of hydrometallurgical methods necessitates a pre-treatment stage that separates the cathodes from the rest of the cell including the current collector. Whereas pyrometallurgy simply crushes or shreds entire batteries regardless of type.

Direct recylcing seeks to address the negatives of pyrometallurgy (low recovery rate, long processing time, high energy consumption and significant greenhouse gas emissions) and hydrometallurgy (treatment complexity, high costs, and heavy water consumption). To this end, direct recylcing seeks to preserve the underlying structure of

electrodes and directly repair or replace any losses to active material (i.e., Li). This greatly reduces input costs because it does not extract the valuable metals but instead maintains and repairs the existing crystal structure. However, it does share commonalities with hydrometallurgy as it requires a pre-treatment separation phase and is also highly customizable for specific electrode chemistries. Numerous challenges remain for the wide scale adaptation process including universality and operational complexity. This dissertation addresses both a pre-treatment process that does not require electrode separation from the current collector and a direct slurry application via plasma treatment.

1.4. ORGANIZATION

The introduction (1.1-1.3) essential background information and the objectives for this Ph.D. research. While the details of this research are presented in the accompanying papers.

Paper I presents a novel charging algorithm that adjusts current based on state of charge and Li-ion diffusivity. This enhances charging rate while degradation is limited via the prevention of crack propagation. Since actual critical fractures stresses are difficult to determine, a maximum stress is used at the limit.

Paper II shows the development of a facile direct recycling methodology for NMC cathodes and MCMB anodes. It seeks to determine which treatment steps are most critical to restoring performance to spent electrodes while also optimizing the process.

1.5. NOVELTY

Paper I introduces a novel charging methodology that greatly uses constant gradient to control the current and degradation. This method creates a constant gradient at the electrode surface which serves to prevent crack propagation while exploiting variable diffusivity to adjust the current. Thus, higher currents can be applied at high diffusivity and lower currents at low diffusivity preventing the buildup of stress due to the concentration gradient. This charging approach combines the best of both worlds by significantly curtailing degradation rate while greatly reducing charging time.

Paper II shows the development of direct recylcing remanufacturing process with a degree of universality as it is effective on both NMC-622 cathodes and MCMB anodes. However, the central innovation is the combination of plasma treatment to scour the surface of the degraded electrodes clean and direct slurry application on electrodes still attached to their current collectors. This two-step process maintains and repairs the structural integrity of the existing material with NMC-622 cathodes being further enhanced by a Relithiation step. This combines to create a facile process that does not require high temperatures, complicated chemistries or separation which greatly limits the creation of toxic byproducts, contaminated wastewater and greenhouse gas emissions.

PAPER

I. OPTIMAL CHARGING FOR BATTERY LONGEVITY THROUGH CONTROLLED LITHIUM CONCENTRATION GRADIENT

Kaz Adewuyi[1], Kiernan O'Boyle[1], Hiep Pham[1], Robert Landers[2], Jonghyun Park[1]*

[1]Department of Mechanical and Aerospace Engineering, Missouri University of Science and Technology, Rolla, MO 65409-0050

[2]Department of Mechanical Engineering, Notre Dame University

ABSTRACT

One of the key challenges in battery degradation is mechanical failure, such as cracks and delamination, caused by stress from lithium concentration gradients inside active particles. The most crucial factor in crack propagation is the maximum stress experienced by the material, as cracks initiate and propagate when the stress exceeds the material's strength. In conventional charging protocols, such as constant current constant voltage (CCCV) charging, the concentration gradient and corresponding stress levels vary, and reaching critical levels can lead to mechanical failure. This paper introduces a new optimal charging methodology called constant gradient constant voltage (CGCV), which regulates the charging current to maintain a constant lithium gradient at the surface of active particles, thereby limiting stress development and mechanical crack propagation. To control the concentration gradient, factors such as charging current, lithium diffusivity, and particle geometry must be considered. However, since diffusivity is state-of-charge (SOC)

dependent and difficult to measure in real-time, a model is employed to create the charging protocol.

Two gradient options, mid and high, are considered by setting the maximum stress limit relative to the 0.1C CCCV condition. Two scenarios have been demonstrated. In the first scenario, the CGCV shows a significant reduction in charging time, with a 56% (High CGCV) or 49% (Mid CGCV) reduction compared to CCCV, while exhibiting slightly slower degradation rates. In the second scenario, 0.5C CCCV, which has a roughly equivalent charging time to High CGCV, shows significantly more capacity fade than High CGCV; it takes 66 cycles for 20% capacity fade, while High CGCV takes 100 cycles to reach only a 12% capacity fade. Additionally, it exceeds the capacity fade of High CGCV after only 36 cycles. These two scenarios show that the CGCV methodology efficiently mitigates degradation while shortening charging time. This new protocol may hold great potential for addressing the key challenge of regulating battery degradation during fast charging.

1. INTRODUCTION

Lithium-ion batteries (LIBs) are an important class of batteries due to their high power and energy densities, as well as their versatility as energy storage devices for applications ranging from small portable electronics to electric vehicles (EVs) [1]. Energy efficient vehicles are of vital importance because transportation accounts for 30% of America’s total energy usage and 70% of its petroleum consumption. Additionally, EVs have significant environmental and health advantages as they reduce greenhouse gas and

particulate emissions which cause cancer, cardiovascular, respiratory, and reproductive issues. Despite their numerous advantages, EV's lag behind conventional automobiles when it comes to fueling time. Thus, lowering charging time below 6 mins serves a major goal for wider scale EV adaptation However, massive reductions in charging time can accelerate cell degradation such as Li plating, dendritic growth, thermal runaway, crack propagation, Li isolation, and separation of electrode from current collector [2, 3]. Therefore, a balancing act must be struck that lowers charging time while maintaining long term cell performance.

Battery charging performance can be enhanced through several approaches. First, the battery itself can be modified by enhancing cell material properties and optimizing electrode design. This broad category includes improvements to electrolytes, electrodes, binders, cell architecture, etc. For example, high concentration lithium bis(fluorosulfonyl)imide/1,2-dimethoxyethane LiFSI/DME electrolytes, which are organic ethers, can boost charging times of 70% capacity in 30 min with no plating [4]. This high ionic conductivity allows for rapid transfer of Li ions between the electrodes. In electrodes, the primary properties relevant to fast charging are reaction kinetics, diffusion lengths, electrode crystal structures for Li-ion transfer, ionic diffusivity, and electrical conductivity [2]. Typically, cathodes are spinel oxides, layered oxides, and olivine polyanions. Their unique crystal structures determine the best pathways for optimization [5]. For example, spinel oxides allow fast Li-ion transport because their 3D pathways allow omnidirectional ion movement unlike layered oxides which only have bidirectional movement. These unique properties from the spinel crystal structure can be enhanced via doping where 5%

Ru doping of $LiNi_{0.5}Mn_{1.5}O_4$ boosts the electronic conductivity by 100% and diffusivity by an order of magnitude [2].

Another major approach enhances charging performance with control-based techniques that manage the battery system directly. For instance, a feedback loop can reduce constant current constant voltage (CCCV) charging time by maximizing charging time in CC and thus minimizing the CV region [6]. In CCCV, the CC regime charges a battery at a set current until a maximum voltage dependent on battery chemistry is reached. The CV regime holds the voltage constant by reducing the current until a minimum current cutoff or set amount of time has passed. Another approach is to use a built-in resister as a compensator which allows for dynamic updates by estimating the internal resistance of the cell. This method extends time spent in the CC regime by 40%, reducing the overall charging time by limiting time spent in CV [7, 8]. These resistance measurements allow for adjustments after every cycle by indirectly accounting for the internal cell dynamics, mainly degradation rate. The simplest version uses a digital controller to switch between CC and CV when a preset voltage is reached. Switches occur more frequently as cycle life increases due to further degradation and current is not directly accounted for. More advanced active feedback control can be achieved using software and/or hardware solutions. Software approaches have broader applications across various battery types. The digital control technique allows batteries to run both CC and CV without current feedback which reduces both cost and system complexity [9]. Alternatively, the charger with a flyback converter can use a discontinuous conducting mode where a secondary diode limits peak current and allows for an additional CC step at a different current value [10].

Lastly, developing a new charging methodology is advantageous because it is independent of cell design and can be applied universally across different cell designs. All charging methodologies have a tradeoff between charging rate and degradation rate. However, any new method must be superior to CCCV in either or both metrics for adoption [11]. Two such charging solutions are Multistage Constant Current (MCC) or step charging and Constant Power (CP) methodologies. The broad MCC methodology combines charging, discharging and resting steps at different currents and periods with transitions triggered by time cutoffs or voltage constraints [12]. This allows for it to be highly customizable and optimizable, but the simplest MCC has two steps usually with higher current first and lower current second. The CP methodology also starts with a high current and keeps power constant by gradually reducing the current until a voltage cutoff is reached. Since high current at higher SOC leads to lithium plating, this method prevents the plating problem by lowering current at higher SOC. One study determined that for $LiCoO_2$ with CC cutoff of 4.2 V that the order of capacity fade after 100 cycles to be CP > MCC > CC for low C-rates (i.e., 0.5C) [12]. While at higher C-rates (i.e., 1.0C), the order changes to MCC as the highest and CP as the lowest [12]. C-rates are defined as a ratio between charging time and current that tells how long it takes a cell to fully charge or discharge under ideal conditions. For instance, a C-rate of 1C should charge or discharge a cell in one hour.

Another strategy is to create steps based on the cell's internal resistance. For lithium iron phosphate (LFP) batteries, 10 A was applied until 70% state of charge (SOC) followed by 2 A until the voltage cutoff. This approach reduced charging time by 20% while the

combination of higher current at low to mid SOC and lower current at high SOC minimizing lithium plating [13].

While MCC or multistep (MS) is the most common solution, there exists additional methods such as pulse charging (PC) and voltage trajectory (VT). Pulse charging alternates between a higher current charging period and a second period which can be lower current charging, lower current discharging or a rest period. This process reduces polarization because the concentration gradient doesn't build up during the second period. Voltage Traectory is similar to the aforementioned CP methodology where the current starts high and ends low while being adjusted to limit impedenace. One paper seeked to compared these more complex approaches to the standard CC and MS methodologies. Here, CC was set to 2C (86 A), and MS started at 2.5C and dropped to 0.5C by .25C per step at different voltage switch values. PC combined 2.5C charging periods with rest periods and VT started at 2.5C while adjusting the current down based on impedance. At room temperature, there was minimal difference in charging capacity or final charging time. However, MS did the best job minimizing time spent in CV while PS was ineffective at reducing charging time. However, they didn't examine degradation across multiple cycles for this process so some improvements might be hidden [14].

These charging methodologies have demonstrated improved charging time or cycle life; however, they do not directly address specific degradation mechanisms. In particular, there is no effort to mitigate mechanical degradation, which is a critical factor associated with fast charging. The extraction and insertion of ions distorts the structure of the electrodes. Analysis via TEM has shown that if there is insufficient time for the ions to diffuse through the electrode, inhomogeneity results in stress buildup which is relieved by

fracturing [15]. This means that stress can freely build up until a critical fracture point is reached after which cell degradation occurs. Modelling of $LiCoO_2$ shows that a critical fracture point is determined by particle size, diffusivity, and current rate by solving the elastic boundary conditions [15]. Therefore, the main method to prevent crack propogation is to lower the critical facture energy by reducing the particle size or the C-rate. This model determines critical particle size is 250 nm at 2C and decreases to 190 nm at 6C during discharge. Another important factor to consider is if any phase shift occurs for the electrode particles.

For instance, studying $LiMn_2O_4$ shows that if Jahn-teller distortion occurs during the transition from spinel to cubic then fracture is unavoidable [16]. This occurs due to the mismatch in lattice parameters between the two crystal structures causing an immediate stress high enough to induce fracture. This region can be avoided for particles between 500 nm to 800 nm during charging if the cell is kept above 3 V. However, if the particle is kept in single phase then fracture tends to occur in 4 V plateau region if current exceeds 5.36 C for 5 nm particles [16]. Though lesser subcritical fracturing can occur due to surface interactions between cracks and the electrolyte due to natural wear and tear [17, 18].

Mechanical degradation, resulting from volume changes during lithium intercalation and deintercalation into the cathode during charging and discharging, is a significant battery degradation mechanism. This work proposes a new optimal charging methodology which addresses this issue by managing two crucial factors: the lithium concentration gradient in the active particles and the charging time. Electrodes often have microscopic cracks, and these cracks are less likely to grow when the stress caused by the gradient of lithium-ion distribution is lower than the fracture energy of the material. This

gradient is influenced by the relationship between the diffusivity of lithium ions and the flux during charging and discharging. Since the diffusivity is strongly dependent on SOC, the idea is regulating the gradient by varying the current based on this SOC dependent diffusivity. Specifically, the concentration gradient is controlled and is fixed to a certain value before the CV profile. This is called Constant Gradient (CG), which is designed to allow higher current input during the high diffusivity SOC regions, while minimizing the stress development in the low diffusivity regions by using a smaller current input.

2. EXPERIMENTAL DESIGN & CONSTANT GRADIENT CHARGING METHODOLOGY

The maximum stress in a particle is directly related to the maximum concentration gradient of Li-ions at the surface. Thus, the proposed charging methodology in this paper generates a current profile that maintains a constant concentration gradient throughout the entire operation. Figures 1(a) and (b) illustrate Li-ion flux into two crystal structures, one with low diffusivity and one with high diffusivity. The concentration distribution and its gradient are strongly dependent on the diffusivity. As shown in Figure 1, lower diffusivity creates a higher lithium concentration gradient given the same Li-ion flux. Figure 1(c) shows a battery response from a pseudo-2D battery model with a variable diffusivity. The blue line is the concentration gradient at the particle surface, while the red line is the particle diffusivity. This figure illustrates that the concentration gradient is strongly affected by diffusivity and increases for low diffusivity. At high concentration gradient but low diffusivity (a) , an uneven distribution of Li ions occurs as they attempt to rush into the matrix. However, with low concentration and high diffusivity (b) an orderly even flow

of Li ions into the matrix is observed. Finally, the last part shows that diffusivity and concentration are inversely related as at constant current. High concentration means low diffusivity in a system exposed to constant current.

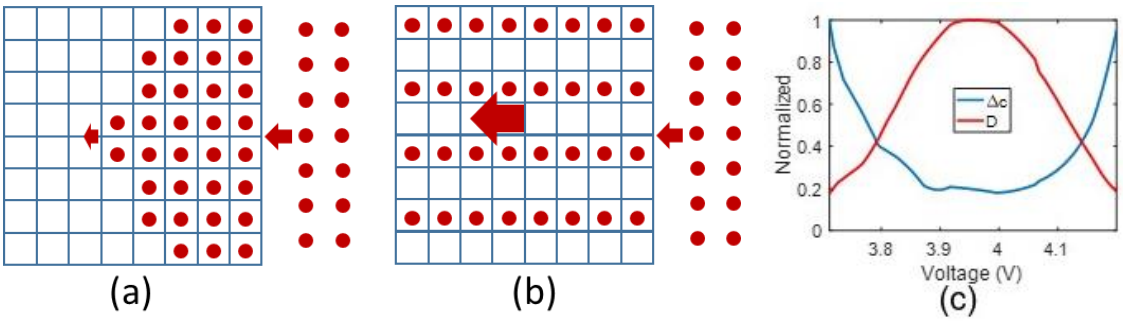

Figure 1: High concentration gradient at low diffusivity (a), and low concentration gradient at high diffusivity (b). Simulated concentration gradient (Δc) and diffusivity (D) as a function of voltage (c).

Motivated by this correlation, we have developed a constant gradient charging algorithm with the objective of maintaining a consistent concentration gradient at the surface of particles. This algorithm leverages the relationship among input current, diffusivity, and concentration gradient, which can be derived from Fick's law. The subsequent inquiry pertains to the determination of the specific value to be maintained. To address this, two scenarios have been delineated: one aims for stress development equivalent to that of CCCV charging but with expedited charging times, while the other targets similar charging durations to CCCV but with reduced degradation. To ascertain the reference concentration gradient for these scenarios, we employ a model based on 0.1C CCCV conditions. Within this framework, the peak stress during CCCV is estimated, and the resulting concentration gradient serves as the reference benchmark.

2.1. EXPERIMENTAL DESIGN

In this work, $LiMn_2O_4$ (LMO)-based half cells are used. These coin cells are fabricated with LMO paste using 85.5 wt% LMO powder (MTI, 13 μm average radius), 6.5 wt% carbon black (CB, Alfa Aesar) and 8 wt% Polyvinylidene fluoride (PvdF, Sigma-Aldrich) dispersed in N-Methyl-2-pyrrolidone solvent (NMP, Sigma-Aldrich). The coin cells are assembled in an argon-filled glove box with a PP/PE/PP membrane (Celgard) as the separator. All experimental testing is done using Neware II Battery Testers. These cells were subjected to a minimum of 10 charge/discharge cycles at 0.1C between minimum and maximum voltages of 3.0 and 4.2 V, respectively, during formation cycling. The nominal capacity of the electrode material from the vendor is 120 $mAhg^{-1}$. All usable fabricated cells have a final specific capacity above 90 $mAhg^{-1}$ and the last two consecutive columbic efficiency cycles are required to be above 97% with a difference of less than 1.0%. The masses vary from 8.1-10 mg with the median mass of 9.1 mg.

Two cells were subjected to a constant current of 0.01C and the resulting OCV curve is shown in Figure 3. These cells also undergo GITT testing where the current is 0.1C (0.094 mA) for charge or discharge periods of ten minutes followed by ten minutes of relaxation with the resulting diffusivity profile shown in Figure 3. The fabricated coin cells are randomly assigned for CCCV and CGCV charging methodologies. The CV region starts once 4.2 V is reached and ceases for all charging methodologies once the current reaches 0.01C. The battery parameters used for the simulations conducted in this paper are given in Table 1 with the parameters provided by measurements of our cathodes clearly denoted with a star.

Table 1: Single particle model parameters [26, 27].

Parameter	Value
LMO thickness (cathode), l_p *	40-60 μm
LMO size (cathode particle size), R_p *	14 μm
Reaction rate coefficient for positive electrode, k_p	2×10^{-6} $m^{2.5}mol^{-0.5}s^{-1}$
Solid phase lithium ion diffusivity (cathode), D_p	1×10^{-13} m^2/s
Maximum solid phase concentration (cathode), $c_{s,max}$	22860 mol/m^3
Electrolyte concentration, c_e	2000 mol/m^3
Electrolyte phase volume fraction (cathode), ε_{ep}	0.444 (0.3–0.6)
Solid phase volume fraction (cathode), ε_{sp}	$1 - \varepsilon_{ep} - 0.259$
Cathodic charge transfer coefficient,	0.5
Cell resistance, R_{cell}	0.01 Ω

*measured values

2.2. OCV & DIFFUSIVITY CONVERSION

To generate constant gradient profiles, OCV and Diffusivity curves must be acquired and put in terms with respect to SOC which ranges from 0 to 1. OCV curves are constructed by charging and discharging cells using a very low current (0.01C). Since the applied current is low, the voltage can be assumed to cover the full range. Therefore, voltage at the start of cycle is assigned an SOC of 0 and at the end 1. All other voltage points use time to interpolate a corresponding SOC value. Sufficiently low current charging can be assumed to cover the entire capacity range of a given cell. The SOC is given more generally by equation (1) which is provided below

$$SOC(t) = \frac{Cap(t)}{Cap_{total}} \quad (1)$$

where *Cap(t)* is the measured capacity at a given point in time using Coulomb counting at a given point and Cap_{total} is the total capacity of the OCV profile. Next, run the cell used for OCV at 0.1C to provide an experimental voltage profile. Now, run a Single Particle (SP) model as described in the addendum at 0.1C using constant diffusivity. An initial SOC value will be needed to match the model to experimental. This is because the cell cannot be assumed to be fully charged or discharged at higher C-Rates. The selected starting SOC minimizes the Normalized Sum of Square Errors (NSSE) given by equation (2)

$$NSSE = \frac{1}{n}\sum_{i+1}^{n}\left(V_{sim} - V_{cell}\right)^2 \quad (2)$$

where *n* is the number of data points, V_{sim} is simulated voltage and V_{cell} is experimental cell voltage. Thus, the OCV curves have been converted into terms of Voltage and SOC.

The next step is to generate a diffusivity curve that is also in terms of diffusivity and SOC. Diffusivity is measured using the Galvanostatic Intermittent Titration Technique (GITT) which utilizes an alternating series of current pulses (i.e., charge or discharge) with constant current periods and relaxation periods with no current (i.e., rest periods). This technique is applied to the same cells used to generate OCV curves. A full GITT cycle consists of charging and relaxing the battery until a maximum voltage is reached and then discharging and relaxing the battery until a minimum voltage is reached. The cell is charged between upper and lower voltage limits based on the cathode and anode material properties. The charge and discharge pulse periods are selected such that the voltage achieves a linear steady-state response, and the relaxation pulse periods are selected such that the battery voltage equilibrates. The current pulse and rest periods are characterized by two distinct

regions, one consisting of a fast voltage change and the other consisting of a slow voltage change. Using data from the GITT test, the diffusivity for each charge and discharge is given by equation (3) [28, 29]

$$D = \frac{4}{\pi\tau}\left(\frac{n_m V_m}{S}\right)^2\left(\frac{\Delta E_s}{\Delta E_t}\right)^2 \tag{3}$$

where τ is the current pulse length, n_m is the number of moles in the electrode, V_m is the electrode molar volume, S is the electrode surface area, ΔE_s is the voltage change resulting from the current pulse, and ΔE_t is the voltage change from the last rest to the current rest. The selection parameter is whichever cell has superior coulombic efficiency. Figure 2 illustrates the location of these variables.

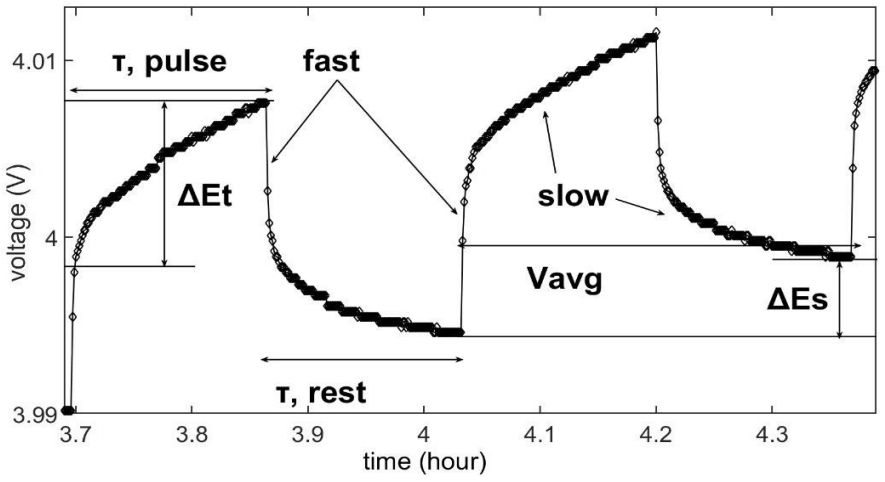

Figure 2: Voltage evolution during GITT cycling.

Now, diffusivity is in terms of average voltage which can be converted into SOC using the OCV curve. Average voltage values can be matched to SOC values from the OCV which converts diffusivity in terms of SOC. Representative OCV and diffusivity

curves as functions of SOC are shown in Figure 3. Diffusivity data points correspond to average voltages shown in Figure 2 and finite diffusivity points given by equation (2). Thus, the conversion from average voltage to state of charge is complete as shown in the figures below for OCV and SOC.

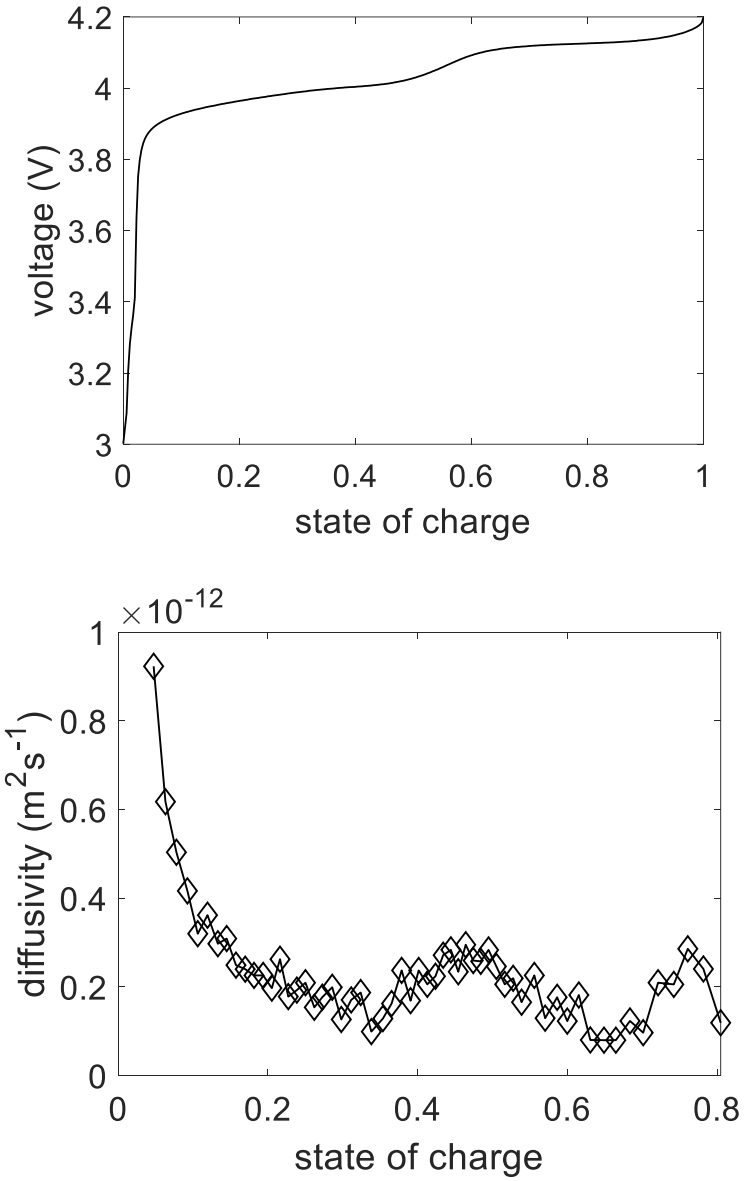

Figure 3: Open circuit voltage versus state of charge (top) and diffusivity versus state of charge (bottom).

Now, with variable diffusivity in terms of SOC and OCV in terms of SOC acquired, the model can proceed to developing the constant gradient methodology using the state of charge and open circuit voltage.

3. CHARGING PROTOCOL AND EXPERIMENTAL RESULTS

The proposed charging profile is composed of two regions: a Constant Gradient (CG) region followed by a Constant Voltage (CV) region. In the CG region the current is adjusted based on a battery model to maintain a constant Li-ion surface concentration gradient as the diffusivity changes. Thus, diffusivity is used to adjust the current to better exploit regions of high diffusivity to increase the charging rate and better limit degradation in regions of low diffusivity.

The range of surface gradient values is determined by running a constant current simulation. The electrode surface gradient is given by equation (4)

$$G(t) = \frac{i(t)}{D(t)\,SlF} \tag{4}$$

where i is the current, D is the electrode diffusivity, S *is* the electrode surface area, l is the electrode active material thickness and F is Faraday's constant. This relationship is derived from Fick's first law of diffusion. The surface stress is given by equation (5) [5].

$$\sigma_t(t) = \frac{\Omega E}{3(1-\nu)}\left(\tilde{c}_{avg}(t) - \tilde{c}_{surf}(t)\right) \tag{5}$$

where Ω is the partial molar volume, E is Young's modulus, ν is Poisson's ratio and $\tilde{c}_k(t) = c_k(t) - c_k(0)$, where k denotes average or surface concentration. Thus, a constant current profile using the single particle model will provide us with the relevant reference

points to tune the constant gradient profile. The critical values for tuning at a given constant current are average gradient, maximum gradient and maximum stress which will be elaborated below. Every change in the given constant current requires these three values to be recalculated.

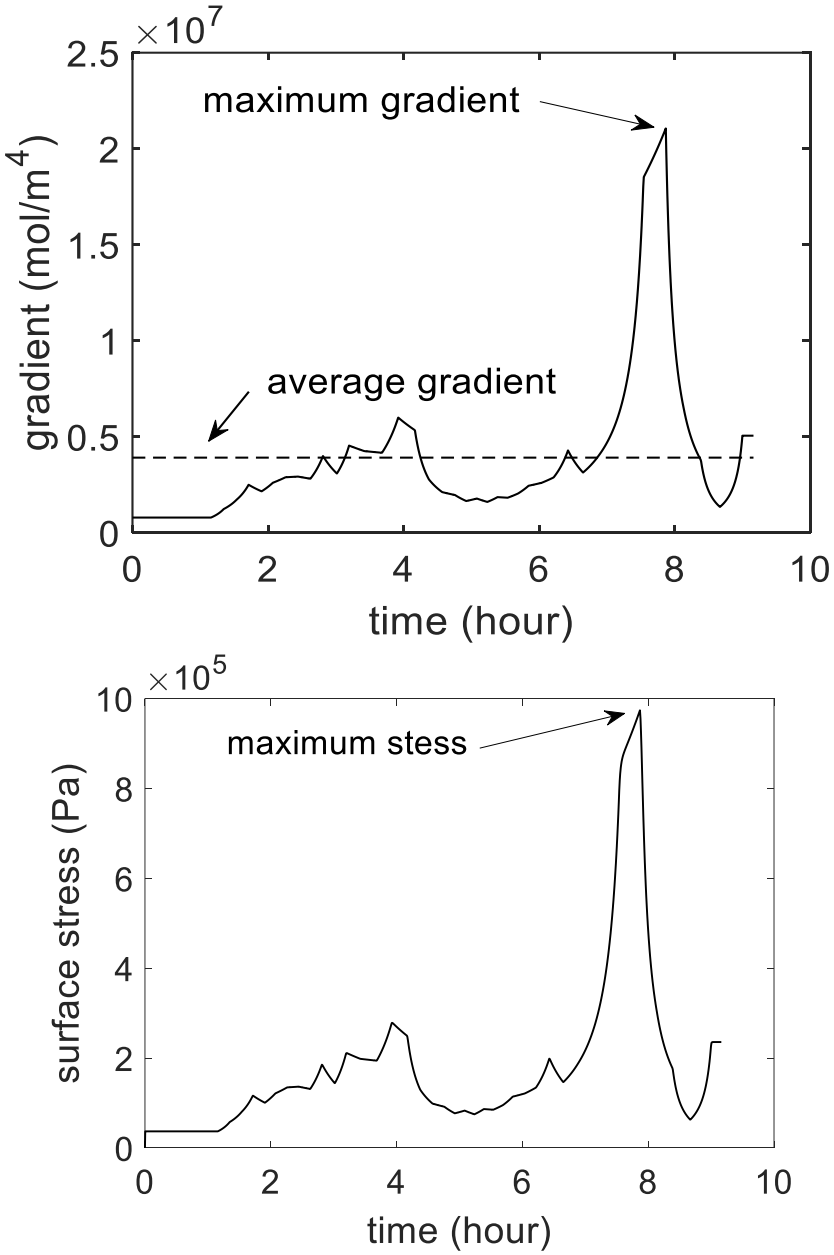

Figure 4: Gradient (top) & stress (bottom) versus time from constant current simulation.

This constant current simulation provides two reference surface gradient values: average (computed over the entire simulation) and maximum (i.e., the surface gradient corresponding to the maximum stress). Figure 4 shows the gradient curve for the simulation and the corresponding stress curve respectively. The average gradient is the lower bound below which any current profile has a longer charging time than that resulting from the constant current simulation. The maximum gradient sets the upper bound such that any gradient greater than this value has a larger maximum stress than the maximum stress resulting from the constant current simulation. The constant gradient current profile is given by modifying equation (4) as a variable diffusivity and a constant gradient are used to set the current, $i(t) = D(t)\, G_{const} SlF$, where G_{const} is a gradient value selected by the user to balance the tradeoff between charging time and degradation rate.

A CC simulation is conducted at 0.1C to determine the maximum surface stress, maximum gradient and average gradient values. This simulation is tuned to match the reference cell by modifying the initial SOC point that the simulation runs from. This simulation gives a maximum stress of 2.97E05 Pa, a maximum gradient of 1.86E07 mol/m^4, and an average gradient of 7.00E06 mol/m^4. The average gradient then has multipliers applied until a CG profile is produced that has maximum stress equal to or barely below 2.97E05 Pa. Note that a multiplier 1.00x will return simulation results nearly identical to that of CC at 0.1C because CG profiles are generated relative to a CC profile. This occurs because the average current at 1.00x will be roughly equivalent to the current at 0.1C. Therefore, signficant reductions in charging time are achievable with multiplers above 2.00x when using constant gradient methodology which are still below the maximum stress limit imposed by 0.1C.

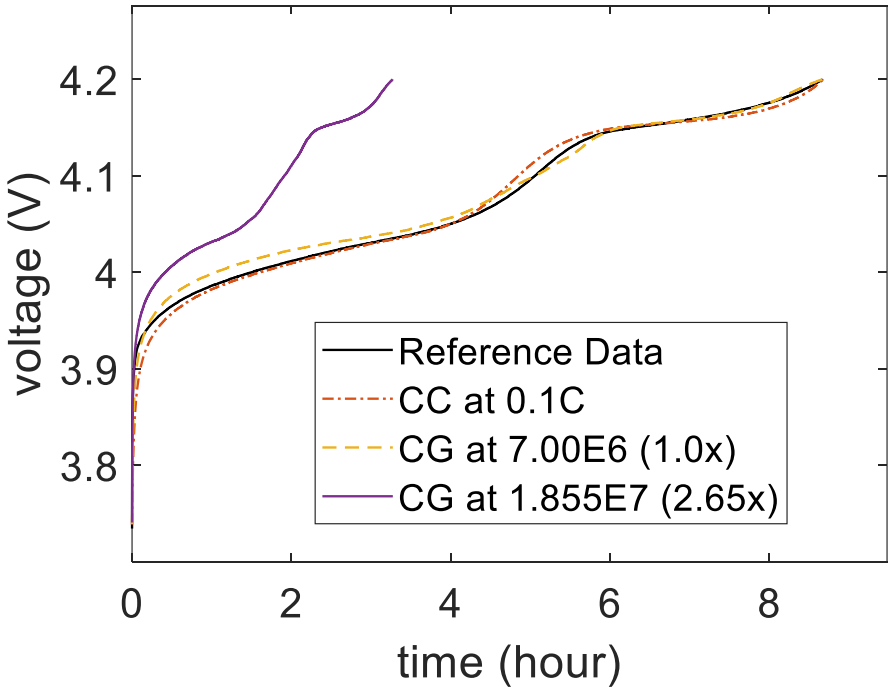

Figure 5: Voltage comparison for multiplier limit.

Figure 5 shows that the highest multiplier is 2.65x which has a maximum stress of 2.95E05 Pa, a maximum gradient of 1.855E07 mol/m^4 and a charge time of 3.271 hours. However, the current profile must be tuned for the battery tester. The simulation has unlimited steps but technically updates every second. However, the battery tester has digital data acquistion limits that prevent the total number of steps from exceeding 250. Therefore, the simulation can only select a number of steps below below 250 while staying below the maximum stress.

If a one second step size is used, there is no significant deviation of the average surface stress which should be held constant under the constant gradient methodology. However, increasing the step size will cause deviations from the average surface stress

which much be properly accounted for when selecting step size. Below the impact of 30, 60 and 90 seconds is observed at different average gradients.

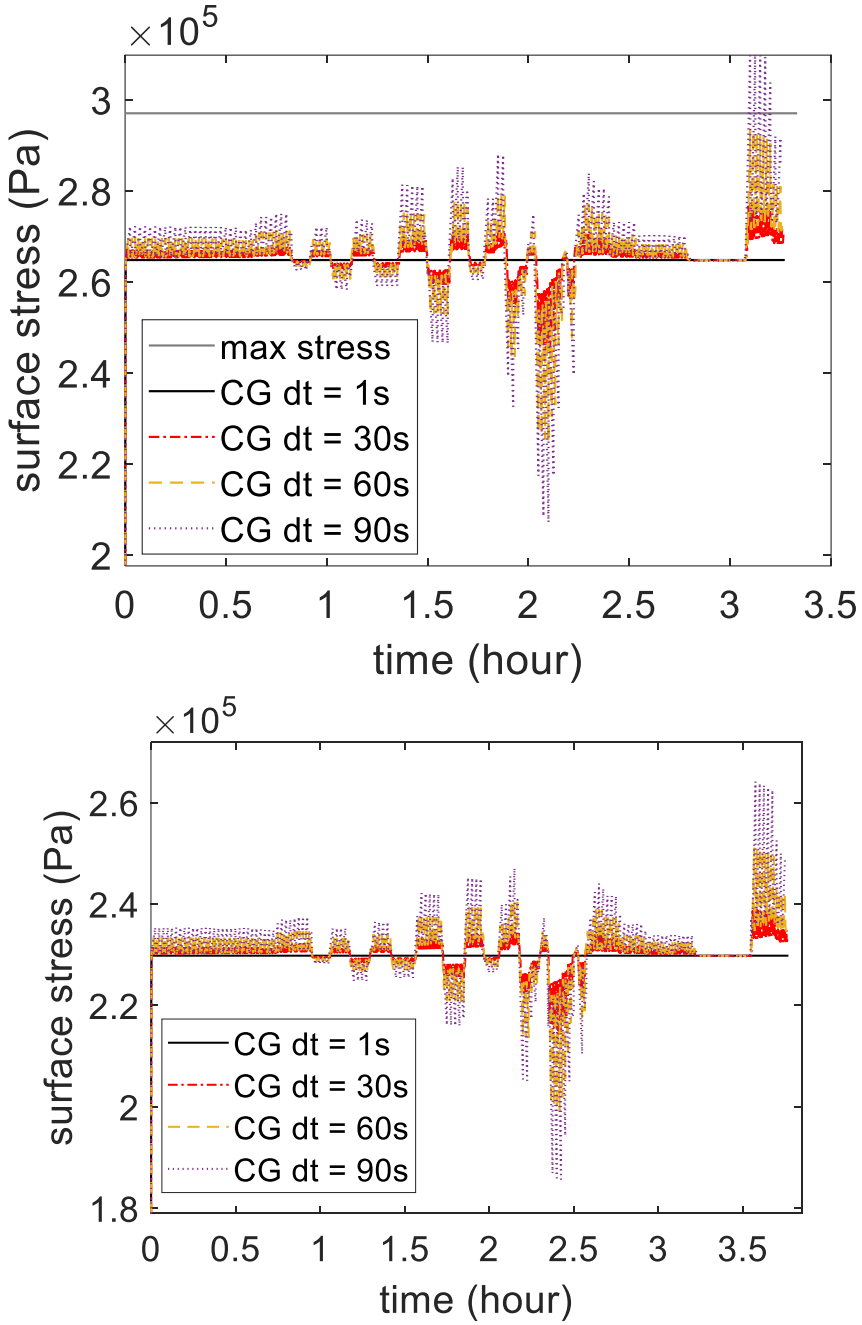

Figure 6: Step size selection (dt) 2.65x (top), 2.30x (middle), and 2.00x (bottom).

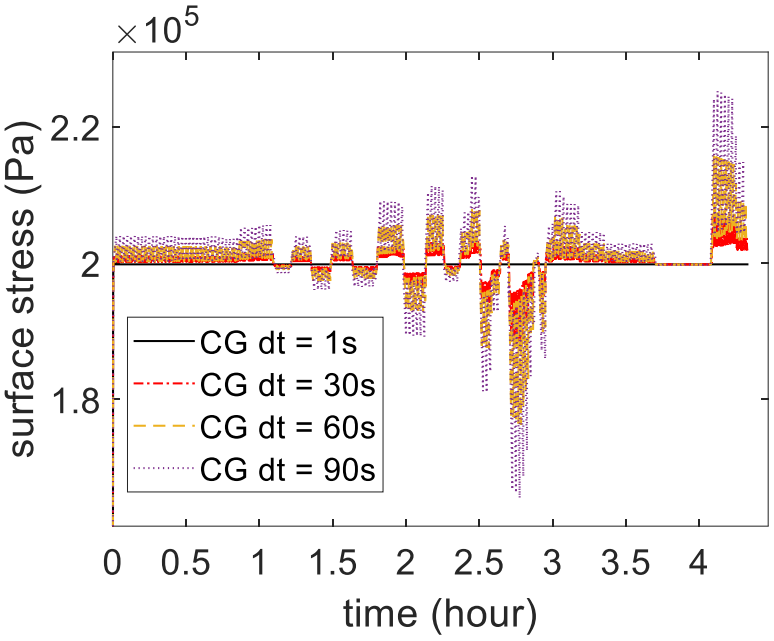

Figure 6: Step size selection (dt) 2.65x (top), 2.30x (middle), and 2.00x (bottom) (cont.).

Figure 6 illustrates the impact of step size and multiplier on stress level. In the model, the step size is updated every second which would create profiles far above the 250 steps allowed. Figure 6 (top) shows that a step size of 90 seconds would exceed the maximum allowable stress level. This would result in faster degradation of the cells relative to constant current. Therefore, we have two methods to avoid this issue which are lowering the multiplier or shrinking the steps. For a gradient multiplier of 2.65x, increasing the step size to 60 seconds puts us below the limit such that slightly slower degredation should occur. If the gradient mutliplier is instead 2.30x, then at a step of 90 seconds, the surface stress would reach above that of 2.65x at 1 second. Ergo, 2.00x is selected because even at steps of 90 seconds, its maximum stress does not reach the 1 second value for 2.65x.

A step size of 60 seconds creates 196 steps and falls below the cutoff of 250 steps for battery tester implementation. The charge time falls slightly to 3.259 hours while the maximum stress is 2.93E05 Pa and gradient at 2.04E07 mol/m^4. This is below the maximum stress limit of 2.97E05 Pa but exceeds the maximum gradient of 1.86E07 mol/m^4 . This means that any step implementation selected will have a lower maximum gradient multiplier compared to the simulation in order to account for stress increases during a step.

3.1. EXPERIMENTAL RESULTS

First, lets analyze two test cells to determine the effectiveness of both step implementations. When properly implemented there should be no large voltage spikes in or trap regions where the current stays in the time period too long appear as troughs and occur when current falls too far between steps.

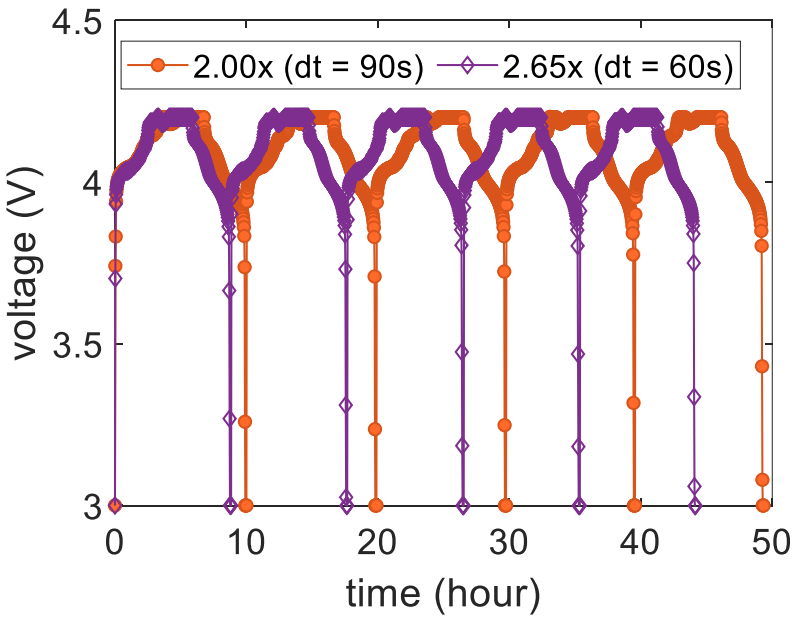

Figure 7: Voltage vs time for average gradient 2.00x & 2.65x.

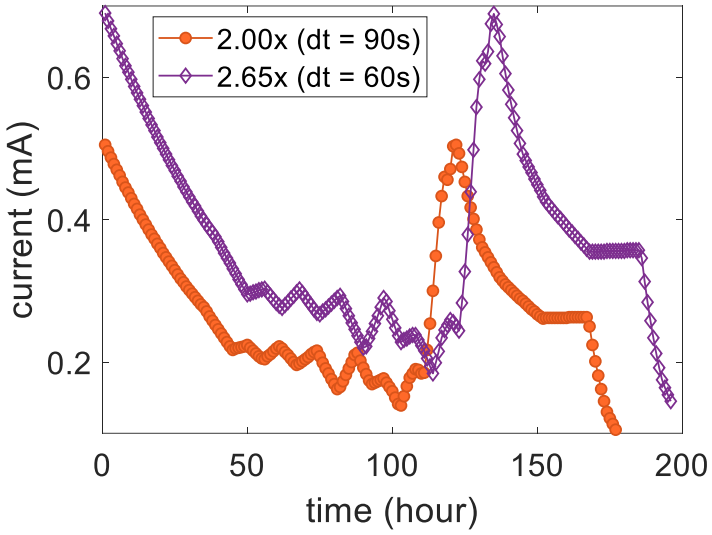

Figure 8: Step current vs time for average gradient 2.00x & 2.65x.

Figure 8 shows the experimental results for an initial test of these step implementations. The step implementation reaches 4.2 V, faster than would be predicted based off the simulation. This is not unexpected given due to cell variance and different environmental conditions. However, the time spent charging during CG is reasonably consistent despite this issue. The cell using a 2.65x gradient multiplier, has an average CG charging time of 3.48 hr experimentally compared to 3.25 hr from simulation (13 min difference). Whereas the Cell using 2.00x has fewer steps (173 to 196) and a lower multiplier experimentally gives an average CG charging time of 4.31 hr compared to simulation at 4.41 hr (5.56 min difference). This cell is below the maximum stress at 2.10E05 Pa (<2.89E05 Pa) and maximum gradient 1.47E07 (<1.81E07). Therefore, less degradation compared to 2.65x combined with a slower charging time is expected for expanded experimental testing. These minimal differences mean that the model is working within reasonable variation. Profiles will be implemented on 15 Cells evenly split between

standard CCCV (CC at 0.1C), low CGCV (2.00x), and high CGCV (2.65x) that all have capacity over 100 mAh/g after formation cycle (charge and discharge 10x). Constant Voltage cutoff occurs at C/100 for all cells.

For our three sets of cells (0.1C CC, Mid CGCV, and High CGCV), the capacity data is normalized to minimize the difference between the cells.

3.1.1. Minimizing Charging Time. First, we will consider an approach focused on minimizing charging time of CG compared to 0.1C CC. This process is relatively simple as applying any multiplier to the average concentration gradient above 1.00x should result in faster charging time due to the higher average current relative to constant current. As shown in Figure 5 above, 1.00x average gradient CG is roughly equivalent in charging time to 0.1C CC. Thus, with our selected multipliers, a significant reduction is expected.

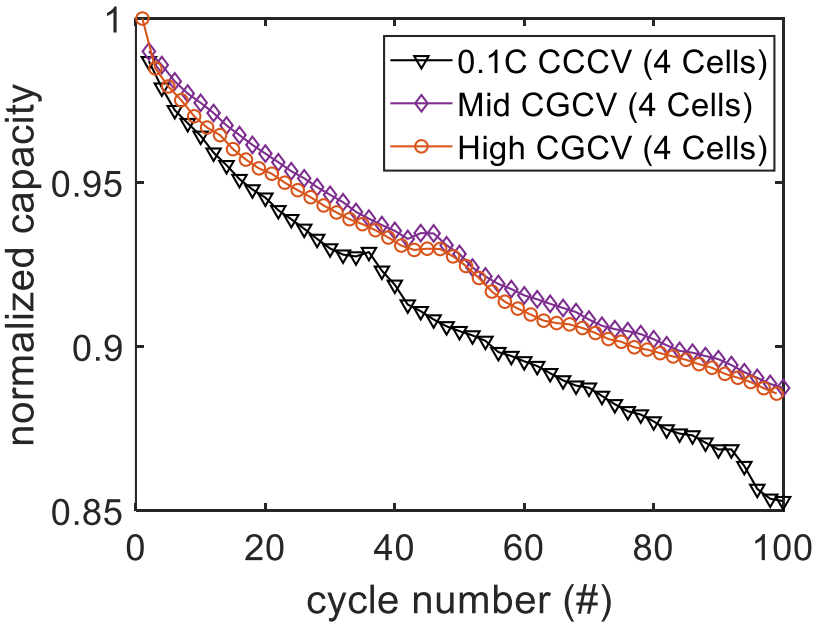

Figure 9: Normalized total charging capacity (top), CC & CG charging capacity (bottom).

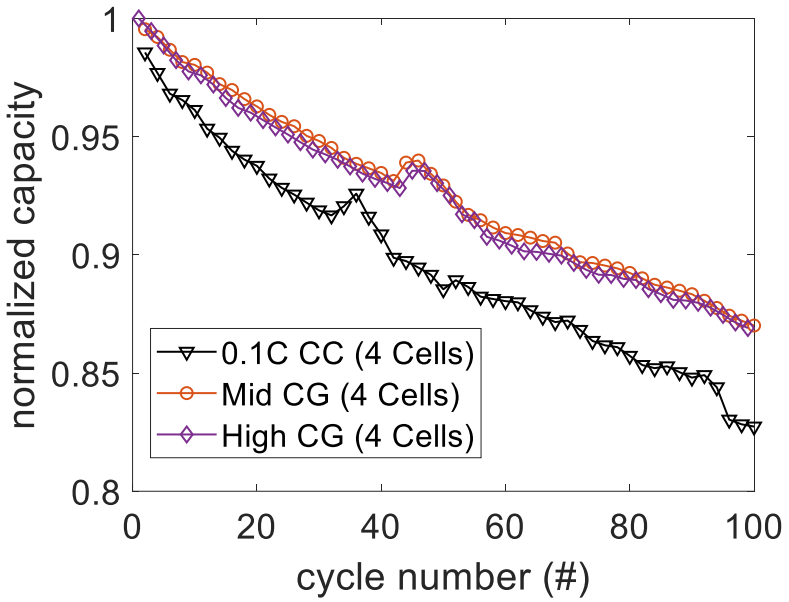

Figure 9: Normalized total charging capacity (top), CC & CG charging capacity (bottom) (cont.).

For Figure 9 (top), 0.1C CCCV has an average normalized capacity of 0.8530 after 100 cycles. While Mid CGCV has an average normalized capacity of 0.8874 after all 100 cycles while High CGCV has an average normalized capacity of 0.8852 after all 100 cycles. Both constant gradient profiles have an average normalized capacity loss per cycle at 0.0011 compared to 0.0015 for CCCV. First, both CGCV profiles show a slower degradation rate than CCCV, although the difference is not substantial at only 0.03. This makes sense as significant degradation is not expected at such a low C-rate. Degradation is still occurring because while CG profiles were selected to be below the maximum stress value of 0.1C, the actual critical stress factor was not calculated so it could still be violated inducing cracking. This is why we can only reduce degradation relative to a reference with CG methodology. Alternatively, this critical stress factor point could not be the dominate force at low currents and instead dissolution or some other form of degradation is most

relevant. Finally, the clear spikes exhibited by all profiles in the late 30s for CCCV and the mid 40s for both CGCV suggest that Jahn-Teller distortion could be occurring due to a phase shift. These spikes occur consistently after roughly 8% capacity loss occurs.

However, let us consider how much the CV regime compensates for any capacity loss. Figure 9 (bottom) shows the results if only the CC or charging time is considered. Here, 0.1C CC has a normalized capacity of 0.8274, Mid CG is 0.8701 and High CG is 0.8617. This increases the average degradation rate to 0.17% (0.15%), 0.13% (0.11%), and 0.14% (0.11%), respectively. Additionally, this shows that overall CV increased the final normalized capacity by 0.0256 for CC, 0.0173 for mid and 0.0235 for high. This relationship makes sense because High CG has a higher maximum stress at 2.93E05 Pa compared to Mid CG at 2.10E5 so Mid CG should be degrading the least. This more clearly illustrates that Mid CG does the best job at reducing degradation without the distortion of CV.

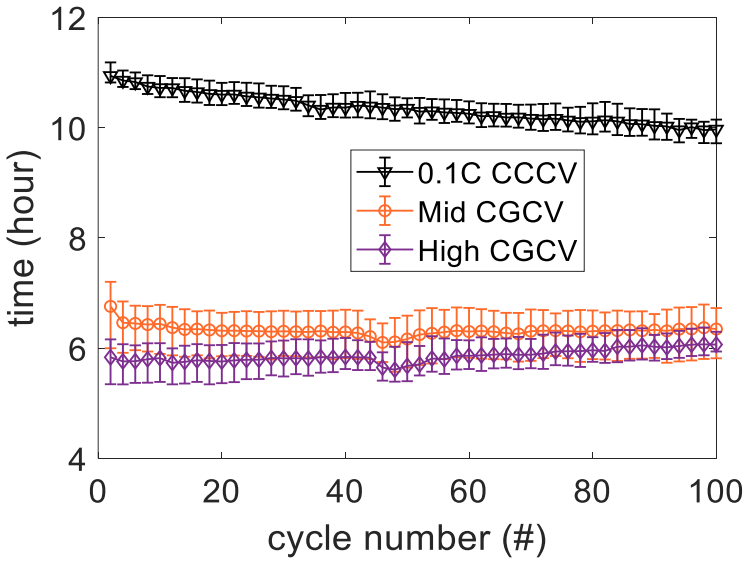

Figure 10: Error plots for total charging time (top), CC or CG charging time (bottom).

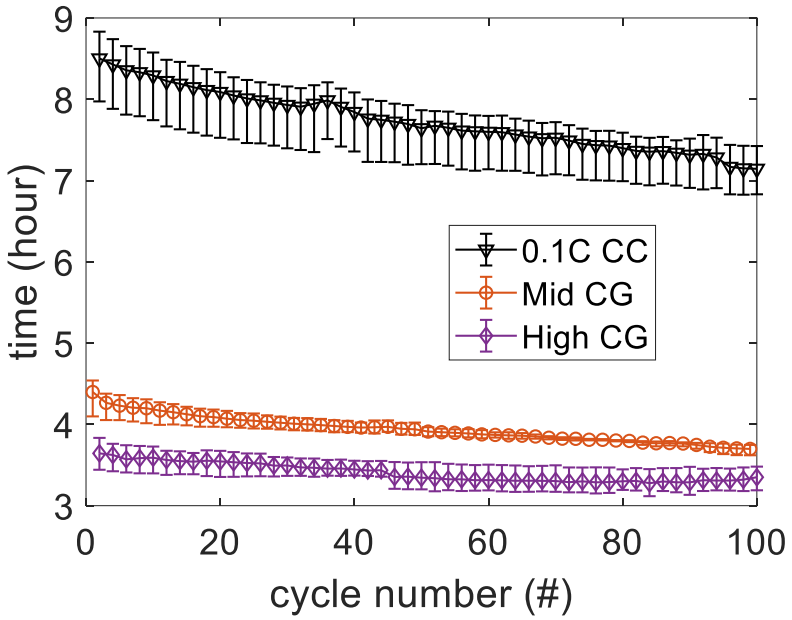

Figure 10: Error plots for total charging time (top), CC or CG charging time (bottom) (cont.).

Figure 10 (top) shows the error plots for charging time for CCCV, Mid CGCV and High CGCV. CCCV has a much higher variance with the average charge time dropping from 11.06 hours to 9.97 hours over 100 cycles. Mid CGCV falls from 6.76 hours to 6.35 hours while High CGCV rises from 5.95 hours to 6.07 hours after all 100 cycles. For CCCV, the charging time drops because less capacity is being reached over the cycle life. There is a limit to how much capacity loss during CC that CV can compensate for. Mid CGCV has similar behavior but a much smaller difference between initial and final charging time. This occurs because Mid CGCV has the slowest degradation and therefore does not benefit as much from additional time spent in CV as performance declines. High CGCV is an outlier and rises slightly because of cell variance as the error bars show that

the maximum value is higher than the minimum after cycle 46. This contrasts with other sets where the minimum value is more dominant.

To explain these phenomena, we must once again consider the impact of constant voltage. Without CV, the CC average charge time drops from 8.63 hours to 7.14 hours while Mid CG falls from 4.40 hours to 3.69 hours and High CG drops from 3.70 hours to 3.35 hours. These charging times all decline because of capacity loss as CV cannot compensate for all the loss during CG or CV. The increase in charging time for High CGCV is shown to be an artifact caused by CV charging. CGCV spends a longer percentage of its total charging time doing CV because as Figure 8 shows, it has a higher final current. The current cutoff point for CV stays constant at 0.002 mA for all profiles which means High CGCV spends the highest percentage of its time running CV.

Thus, High CGCV shows the fastest charging performance and 0.1C CC is the lowest; Mid CGCV has the least degradation and gains the least benefit from CV. Finally, Mid CGCV has the least variance because between cells due to its lower stress value. Since it is further way from the maximum allowable stress, Mid CGCV profiles don't endure as much stress and thus cell variance is less of a factor for its CG charging performance. As shown above in Figure 6, such deviations can be rather significant at High CGCV charging and coin cell variance would exacerbate this issue. The variance is also noted for the CCCV cells.

3.1.2. Minimizing Degradation. The above experiment clearly shows time reduction but the impact of CG profiles on degradation is less clear. However, by raising the CCCV C-rate from 0.1C to 0.5C, total charging time roughly equivalent to High CGCV can be achieved.

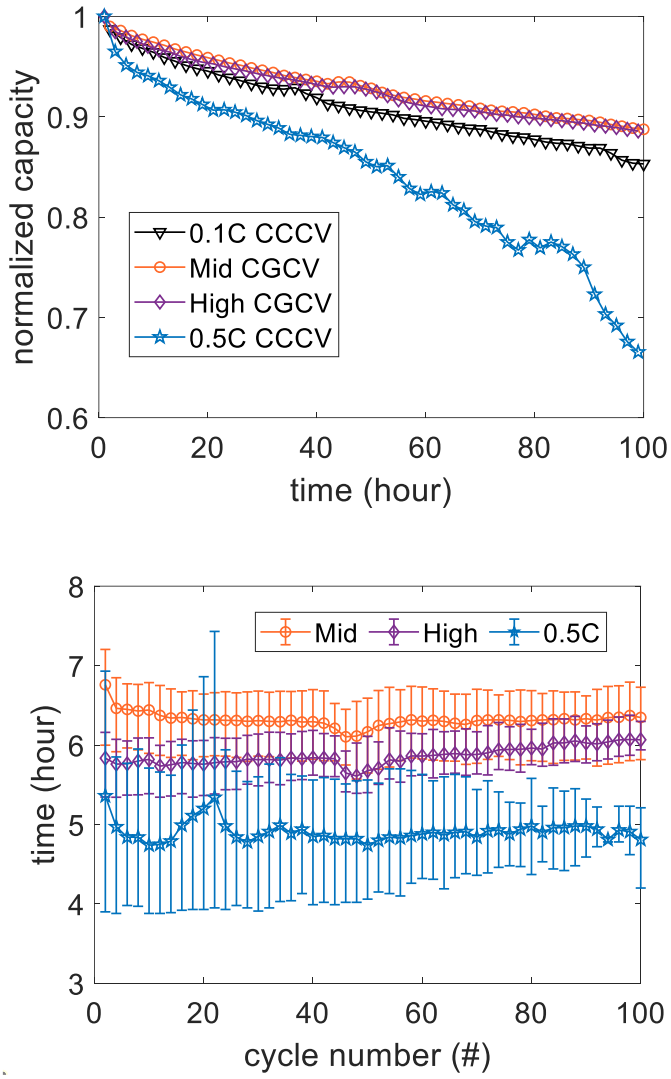

Figure 11: Normalized capacity with 0.5C (top), error plot total charging time (bottom).

The second cycles for High CGCV average 5.91 hours whereas 0.5C CCCV is 5.78 which is approximately a 2 percent variance and can be attributed to cell variability. The second cycle is the relevant comparison because sitting coin cells settle at different initial voltages which distort charging time during their first cycle. Figure 11 (top) shows a clear difference in degradation rate as normalized capacity at 0.5C falls below 0.88 after only the 36th cycle. Neither Mid CGCV nor High CGCV ever falls below 0.88 over 100 cycles.

Furthermore, its final normalized capacity drops to about 0.66 after the full 100 cycles. This means its degradation rate per cycle is at 0.34%, more than double the rate at 0.1C and triple that of Mid and High CG.

Meanwhile Figure 10 (bottom) shows the time evolution. First, 0.5 CCCV has far more error plot variance because the higher current exacerbates difference between cells. The gap between total charging time expands over cycle life as 0.5C CCCV declines to 4.81 from 5.78 hours while High CGCV rises slightly to 6.07 from 5.91 hours. This charging time drop is caused because CV cannot compensate for the rapid decline in normalized capacity.

4. CONCLUSIONS

This paper shows that the proposed new optimal charging methodology called CGCV, which limits mechanical crack propagation at the surface by regulating the current to maintain a constant lithium gradient at the surface is effective. Two scenarios prove that it can significantly reduce charging time and degradation. This first scenario is relative to 0.1C CCCV and shows that High CGCV can reduce total charging time by 44% and CG vs CC charging time by 56%. Mid CGCV reduces total charging time by 39% and CG vs CC charging time by 49%. However, this scenario only shows a minor reduction in degradation at about 3% for both CGCV profiles relative to 0.1C. This necessitated scenario two where cells are cycled at 0.5C to generate total charging time roughly equivalent to High CGCV. This scenario showed rapid degradation with the final capacity fade of both CGCV profiles at about 12% being exceeded in a mere 36 cycles by 0.5C and

20% capacity fade being reached in only 66 cycles. Cells at 0.5C continue to drop precipitously for a final capacity fade of 34% in 100 cycles. Additionally, Mid CGCV produces the lowest amount of variance in time error plots because it does the most to mitigate degradation by being furthest from the maximum stress value and this the critical fracture point.

This new Constant Gradient optimal charging methodology is especially exciting because it can be combined with any control-based solutions while also being usable with any cell design improvements such as doping manipulation or nanostructure design. However, further work is needed to verify that the stress fracture behavior is occurring as predicted. As this paper can only show a relative reduction compared to a reference C-rate.

ADDENDUM: SINGLE PARTICLE MODEL

The SP model is utilized in this work to construct the optimized charging profile because this model is computationally efficient and allows for a fundamental understanding of the chemical interactions that result in changes to concentration, SOC, diffusivity, gradient and surface stress [21-25]. The terminal voltage is the potential difference between the current collectors at the positive and negative electrodes given by

$$V(t) = \phi_{1,p}(t) - \phi_{1,n}(t) \tag{6}$$

where $\phi_{1,p}$ is the cathode solid phase potential and $\phi_{1,n}$ is the anode solid phase potential. The solid phase potential difference is expressed as the overpotential

$$\eta_j(t) = \phi_{1,j}(t) - \phi_{2,j}(t) - U_j(t) \tag{7}$$

where $\phi_{1,j}$ is the solid phase potential, $\phi_{2,j}$ is the solution phase potential and U_j is the OCV, which is a function of concentration. Here, the subscript j is p or n, denoting cathode and anode, respectively. The solution potential difference is

$$\phi_{2,p}(t) - \phi_{2,n}(t) = i(t) R_{cell} \tag{8}$$

where R_{cell} is the electrolyte resistance.

The change in Li-ion concentration inside each electrode is described using Fick's law with spherical coordinates

$$\frac{\partial c_j(r,t)}{\partial t} = \frac{D_j}{r^2} \frac{\partial}{\partial r} \left(r^2 \frac{\partial c_j(r,t)}{\partial r} \right) \tag{9}$$

where c_j is the solid phase L-ion concentration, r is the radial position, t is time and D_j is the solid phase diffusivity. Equation 11 is subject to the following boundary conditions

$$\left(D_j \frac{\partial c_j}{\partial r} \right)_{r=0} = 0 \qquad \left(D_j \frac{\partial c_j}{\partial r} \right)_{r=R_j} = -j_j(t) \tag{10}$$

where the Li-ion molar flux density of the active material at the electrode surface is

$$j_j(t) = \pm \frac{i(t)}{Sa_j l_j F} \tag{11}$$

where l_j is the electrode active material thickness. The sign is negative for the positive electrode and positive for the negative electrode.

The radial dependence of the solid phase concentration in the electrodes is approximated by

$$c_j(r,t) = a(t) + b(t) \left(\frac{r^2}{R_j^2} \right) + c(t) \left(\frac{r^4}{R_j^4} \right) \tag{12}$$

These coefficients are solved by substituting the polynomial approximation in equation (12) into equation (9)

$$a(t) = \frac{39}{4} c_{j,s}(t) - 3R_j \bar{q}_j(t) - \frac{35}{4} c_{j,s}(t)$$
$$b(t) = -35 c_{j,s}(t) + 10R_j \bar{q}_j(t) + 35 c_{j,s}(t)$$
$$c(t) = \frac{105}{4} c_{j,s}(t) - 7R_j \bar{q}_j(t) - \frac{105}{4} c_{j,s}(t) \quad (13)$$

where $\bar{q}(t)$ is the average solid phase flux. The change in average solid phase concentration is

$$\frac{d\bar{c}_j(t)}{dt} = -\frac{3}{R_j} j_j(t) \quad (14)$$

and the change in average solid phase flux is

$$\frac{d\bar{q}_j(t)}{dt} = -\frac{30D_j}{R_j^2} \bar{q}_j(t) - \frac{45}{R_j^2} j_j(t) \quad (15)$$

The surface concentration is

$$c_{j,surf}(t) = \bar{c}_j(t) + \frac{8R_j}{35} \bar{q}_j(t) - \frac{R_j}{35D_j} j_j(t) \quad (16)$$

The SOC is defined as

$$SOC(t) = \frac{\bar{c}_j(t)}{c_{j,\max}} \quad (17)$$

The Butler-Volmer equation relates the flux to the electrode overpotentials

$$j_j(t) = k_j c_{j,\max} c_e^{0.5} \left(1 - x_{j,s}(t)\right)^{0.5} x_{j,s}(t) \left[\exp\left(\frac{0.5F}{RT} \eta_j(t)\right) - \exp\left(-\frac{0.5F}{RT} \eta_j(t)\right)\right] \quad (18)$$

where R is the gas constant, T is temperature, k_j is a reaction constant and c_e is the electrolyte concentration in the solid phase. The model is simplified by treating the temperature, reaction rate and electrolyte concentration as constants. The normalized particle surface concentration is

$$x_{j,surf} = \frac{c_{j,surf}(t)}{c_{j,\max}} \tag{19}$$

where $c_{j,max}$ is the maximum electrode concentration. The terminal voltage is determined using the solid phase potential difference between the electrodes

$$V(t) = U_p\left(x_{s,p}(t), T\right) + \frac{2RT}{F}\left(\ln\left(\frac{\sqrt{m_p^2(t)+4} + m_p(t)}{2}\right)\right) \tag{20}$$

where and m_p and m_n are defined, respectively, as

$$m_p(t) = \frac{i(t)}{Fk_p S_p c_{s,p,\max} c_e^{0.5}\left(1 - x_{s,p}(t)\right)^{0.5} x_{s,p}^{0.5}(t)} \tag{21}$$

ACKNOWLEDGEMENTS

The authors gratefully acknowledge the support for this work by the National Science Foundation (grant CMMI-1538415).

REFERENCES

1. Hinz, H., *Comparison of Lithium-Ion Battery Models for Simulating Storage Systems in Distributed Power Generation.* inventions, 2019. **4**(41).

2. Tang, Y., et al., *Rational material design for ultrafast rechargeable lithium-ion batteries.* Royal Society of Chemistry, 2015. **44**(17): p. 5926-5940.

3. Tomaszewska, A., et al., *Lithium-ion fast charging: a review.* eTransportation, 2019. **1**: p. 1-27.

4. Yamada, Y., et al., *A superconcentrated ether electrolyte for fast-charging Li-ion batteries.* Chemical Communications, 2013. **49**: p. 11194-11196.

5. Miao, Y., et al., *Current Li-Ion Battery Technologies in Electric Vehicles and Opportunities for Advancements.* Energies, 2019. **12**(6): p. 1-20.

6. Cohen, I., *Battery Charging System*, U.S. Patent, Editor. 2020: United States of America.

7. Lin, C.-H., C.-Y. Hsieh, and K.-H. Chen, *A Li-Ion Battery Charger With Smooth Control Circuit and Built-In Resistance Compensator for Achieving Stable and Fast Charging.* IEEE Transactions on Circuits and Systems I: Regular Papers, 2010. **57**(2): p. 506-517.

8. Smith, K.A., C.D. Rahn, and C.-Y. Wang, *Control oriented 1D electrochemical model of lithium ion battery.* Energy Conversion and Management, 2007. **48**(9): p. 2565-2578.

9. Von Novak III, W.H. and L.S. Irish, *Fast battery charging through digital feedback*, U.S.P. Office, Editor. 2017: United States of America.

10. Chen, B.-Y. and Y.-S. Lai, *New Digital-Controlled Technique for Battery Charger With Constant Current and Voltage Control Without Current Feedback.* IEEE TRANSACTIONS ON INDUSTRIAL ELECTRONICS, 2012. **59**(3): p. 1545-1553.

11. Al-karakchi, A., G. Lacey, and G. Putrus, *A method of electric vehicle charging to improve battery life*, in *UPEC 2015*. 2015: Staffordshire University/Stoke-on-Trent, United Kingdom.

12. Zhang, S.S., *The effect of the charging protocol on the cycle life of a Li-ion battery.* Journal of Power Sources, 2006. **161**(2): p. 1385-1391.

13. Anseán, D., et al., *Efficient fast-charging strategies for Li-ion batteries*, in *EVS28 International Electric Vehicle Symposium and Exhibition*. 2015: Kintex, Korea.

14. Mathieu, R., et al., *Electro-Thermal Behavior of Four Fast Charging Protocols for a Lithium-Ion Cell at Different Temperatures,* in *IECON 2018 - 44th Annual Conference of the IEEE Industrial Electronics Society*. 2018: Washington, D.C., USA.

15. Zhao, K., et al., *Fracture of electrodes in lithium-ion batteries caused by fast charging.* Journal of Applied Physics, 2010. **108**(7).

16. Zhang, X., W. Shyy, and A.M. Sastry, *Numerical Simulation of Intercalation-Induced Stress in Li-Ion Battery Electrode Particles.* Journal of The Electrochemical Society, 2007. **154**(12).

17. Li, J., et al., *A single particle model with chemical/mechanical degradation physics for Lithium-ion battery state of health (SOH) estimation.* Applied Energy, 2018. **212**: p. 1178-1190.

18. Li, J., et al., *A single particle model for lithium-ion batteries with electrolyte and stress-enhanced diffusion physics.* Journal of The Electrochemical Society, 2017. **164**(4): p. 874-883.

19. *Galvanostatic Intermittent Titration Technique (GITT)*, M.A. B.V., Editor. 2014.

20. Tang, X.-C., et al., *Capacity intermittent titration technique (CITT): A novel technique for determination of Li+ solid diffusion coefficient of LiMn2O4.* Electrochimica Acta, 2005. **50**(28): p. 5581-5587.

21. Dai, Y., L. Cai, and R.E. White, *Capacity Fade Model for Spinel LiMn2O4 Electrode.* Journal of the Electrochemical Society, 2013. **160**(1): p. 182-190.

22. Lofti, N., *Dissertation: modeling and control of fuel cell-battery hybrid energy sources*, in *Mechanical and Aerospace Engineering*. 2016, Missouri University of Science & Technology: Rolla, Missouri.

23. Marcicki, J., et al., *Design and parametrization analysis of a reduced-order electrochemical model of graphite/LiFePO4 cells for SOC/SOH estimation.* Journal of Power Sources, 2013. **237**: p. 310-324.

24. Prada, E., et al., *Simplified Electrochemical and Thermal Model of LiFePO4-Graphite Li-Ion Batteries for Fast Charge Applications.* Journal of The Electrochemical Society, 2012. **159**(9): p. 1508-1519.

25. Rahimian, S.K., S. Rayman, and R.E. White, Journal of Power Sources, 2011. **196**(20): p. 8450-8462.

II. FACILE REMANUFACTURING AND RELITHIATION FOR SPENT LIHTIUM-ION BATTERY ELECTRODES

Kaz Adewuyi, Kiernan O'Boyle, Tazdik Plateau Patwary, Jonghyun Park*

Department of Mechanical and Aerospace Engineering, Missouri University of Science and Technology, Rolla, MO 65409-0050

ABSTRACT

As the demand for lithium-ion batteries rises, concerns about supply sustainability and environmental impact are growing. Rapidly increasing demand may soon outstrip current lithium reserves. Additionally, landfilling spent batteries poses significant environmental risks, including contamination from toxic heavy metals and organic electrolytes. To address these challenges, battery direct recycling presents a promising solution compared to physical or chemical recycling, which involves high costs, complicated processes, and toxicity issues.

In this work, we present a facile approach to remanufacturing by applying direct recovery principles. Our approach aims to minimize modifications and use the original electrode structure, while restoring the degraded electrode through cleaning, removal, and refilling processes. We employ a plasma treatment and washing process to remove degraded materials, followed by the application of a fresh coat of slurry and a Relithiation process, aiming to restore satisfactory performance to heavily degraded cells. In our investigation, we explore various plasma treatments, the order of treatment steps, types of slurry, and pressing techniques to optimize our process. Together, we incorporate salt

addition to enhance ion conductivity and simplify the drying method using a hot plate and vacuum oven at lower temperatures to mitigate damage to the slurry. These efforts are aimed at improving the overall efficiency and effectiveness of our battery recycling process.

Our investigation reveals that using normal NMC-622 slurry with plasma treatment and pressing yields the best results in terms of cell viability (>80%) and capacity performance restoration for highly degraded cells. To the authors' knowledge, this kind of direct recycling of batteries is being introduced for the first time. This novel approach shows promising results, offering an alternative method for efficient and effective battery recycling.

1. INTRODUCTION

Demand for Lithium-Ion Batteries (LIBs) have skyrocketed over the past decade, primarily driven by Electric Vehicles (EVs) where the global fleet is expected to reach over 7.5 million vehicles by 2030 [1, 2]. Mining operations create numerous environmental and human health impacts through wastewater creation and increase cyanobacteria production [3, 4]. Spent Li batteries, themselves, also create environmental problems if left to sit in landfills due to flammable organic liquid electrolytes and dangerous transition metals [5]. Furthermore, geopolitical concerns emphasize the susceptibility of global supply chains, which has been exacerbated by recent events such as the Covid-19 pandemic and other geopolitical tensions [6]. Recycling used batteries provides a buffer and strengthens energy security in response to these disruptions. Currently, three primary methods for recycling

LIBs are being pursued: pyrometallurgy (physical), hydrometallurgy (chemical), and direct recycling. Pyrometallurgy is the predominant industrial method due to its scalability, simplicity, and broad applicability for mixed cell types. This process involves high temperatures (> 500°C), oxidation, and reduction reactions to recover a mixed metal alloy (such as Co, Ni, Cu, Fe, etc.), which contains the most valuable materials. However, it is characterized by high energy consumption due to the required temperatures and generates hazardous byproducts like toxic gases and side products. Hydrometallurgy, on the other hand, requires advanced knowledge of solution chemistry but offers flexibility to extract pure materials. This method relies on solvent extraction and acid leaching techniques to recover desired materials, often resulting in significant wastewater production. Moreover, hydrometallurgy lacks scalability since cells require careful dismantling to separate components instead of the typical crushing method used in pyrometallurgy. For example, the Umicore method employs a furnace with three major zones to process crushed cells: evaporating organic electrolytes, incinerating plastics, and smelting valuable metals along with waste materials (such as Li, Al, C, etc.) [7, 8]. Whereas the Accurrec method employs a refined form of pyrometallurgy that combines physical and chemical treatments. This method is specifically designed to recover Co and Li from portable LIBs, which are subsequently subjected to a chemical process to extract high-purity metal salts [9-11] . This process involves either direct vacuum distillation for metallic Li or volatilization using a carrier gas for Li oxides.

On the other hand, direct recycling is a remanufacturing approach that seeks to directly recover and repair the active material of electrodes. This differs from the previous pyrometallurgy and hydrometallurgy which fully breakdown electrodes with the aim of

recovery valuable products. Direct recycling is a more environmentally friendly approach that has lower greenhouse gas emissions, water and/or energy consumption than the pyrometallurgy or hydrometallurgy alternatives. In general, direct recycling has three major stages which are shredding/separation, tailored treatment process, and calcination that create a repaired cathode that can assembled into new cells. Separation is the process by which the electrode material is split from the current collector. It is usually achieved via thermal decomposition at high temperature (300-600 °C for 1-2 hours) or dissolution using a highly polar solvent like NMP or DMF to dissolve the binder [11]. Any treatment process is specific to the type of electrode being repaired so it is critical to focus on a specific chemistry.

One novel approach for direct recycling involves immersing degraded LiCoO2 cathodes in various concentrations of Li2SO4 solution (0.1-1 M) with constant currents (-0.12 to -0.42 mA/cm²). The process continues until the cathodic potential stabilizes. The cathode material, which had dropped below 80% of its initial capacity after cycling, is annealed at 700°C for 2 hours, then reduced to powder to form new cathodes. This method restores the capacity performance to 136 mAh/g, close to the practical capacity of 140 mAh/g [12-14]. Another method utilizes redox mediators, specifically 3,5-di-tert-butyl-o-benzoquinone (DTBQ), to deliver Li ions and electrons to relithiate end-of-life NMC111 cathode materials after heat treatment. Experiments with DTBQ concentrations from 0.1 to 0.5 M showed the highest charge capacity at 182.5 mAh/g (initially 183 mAh/g) with the lowest overvoltage, using chemically delithiated NMC111 with 10% capacity loss [15-19]. Another different technique involves a one-step hydrothermal reaction in a Li-containing solution to reconstruct the microphase purity and stoichiometry of LMO

cathodes. Cells cycled between 3.0-4.3 V at C/2 for 200 cycles showed a 20% capacity loss. The cathode strips were harvested, sonicated to remove most materials, and underwent hydrothermal treatment with LiOH at 180°C. This restored the initial capacity to 61 mAh/g and 55 mAh/g after 100 cycles [20-23]. Finally, a simple thermochemical process regenerates NCM523 using molten salts. The spent material is separated from the foil, filtered, and dried. A mixture of NCM523/KCl/KNO3/LiNO3 is heated at 750°C for 12 hours. LiNO3 is added to recover stoichiometric Li content and consume reductive impurities, while KNO3 and KCl stabilize the reaction. This process recovers the capacity of spent NCM523 to 160 mAh/g at 0.2 C, compared to 200 mAh/g for pristine NCM523 [24-27].

In this paper, we introduce several novel elements that set it apart from these traditional recycling methods. Unlike conventional physical and chemical methodologies, which often suffer from high costs, complicated processes, and safety concerns due to waste products and the release of dangerous chemicals, our method focuses on direct recycling. This strategy preserves the critical underlying structures of electrode materials, essential for their effectiveness. Our simplified direct recovery remanufacturing process is designed to reduce operational complexity and expenses. By avoiding the reliance on complicated chemistry and high temperatures (above 500°C), we maintain the vital crystal structure of the electrodes, which is often destroyed in other methods when electrodes are reduced to slag or converted back into precipitate powder through hydrometallurgical approaches. Safety is another significant advantage of our method. By minimizing the release of dangerous chemicals and addressing the safety concerns related to waste products, we enhance the overall safety of the recycling process. This focus on safety,

combined with cost reduction and process simplification, makes our approach highly advantageous.

A key innovation in our process is the inclusion of a plasma treatment step, followed by surface crack filling using fresh slurry. This unique step helps maintain the structural integrity of the electrodes, ensuring their continued effectiveness. Our comprehensive remanufacturing process begins with dismantling the cells and visually inspecting the surface for damage. The cells then undergo plasma treatment and washing, followed by drying and surface treatment to fill in any cracks. After another drying phase, the treated electrodes are reassembled into half cells with Li foil or as full cells. For treated cathodes, we include a Relithiation step to restore their lithium content. Finally, these cells undergo a formation cycle, after which further testing can be applied to ensure their performance. This method is applicable to both anode and cathode electrodes, broadening its utility and scope. By combining these innovative steps into a single, streamlined process, we achieve a novel recycling methodology that not only reduces costs and enhances safety but also preserves the crucial structural features of the electrode materials, extending their usable life and effectiveness.

2. EXPERIMENTAL METHOD

Our process begins with initial cell characterization, where a baseline capacity is determined. This characterization process (capacity/voltage check) is critical because old cells have unknown levels of degradation. Cells are cycled between 2.8 V to 4.2 V for five cycles at 0.1C to stabilize performance, allowing us to categorize cells as ‘Good’ (above

70% practical capacity), ‘Moderate’ (between 70% to 30%), ‘Poor’ (below 30% but above 0), and ‘Zero’ (flatlined or trapped cells). Most cells fall into the ‘Poor’ or ‘Zero’ categories, where the bulk of testing is focused. Next, the cell is disassembled, separating the constituent components (casing, electrodes, separator, spacer, and spring). The separation process is delicate, using a crimping device to open the cell and carefully remove the anode and separator to avoid damaging the cathode. The electrodes are visually classified based on surface damage, ranging from ‘Minimal’ (a few minor pockmarks), ‘Moderate’ (between minimal and significant), to ‘Significant’ (substantial surface loss around 50%). Delamination is always classified as Significant. Figures 1 illustrate various examples of cell damage.

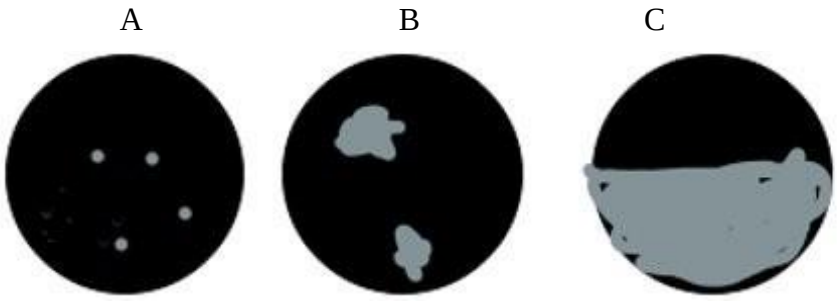

Figure 1: Minimal (A), moderate (B), significant (C) examples [black: electrode part, gray: exposed current collector].

Plasma treatment follows, using an oxygen environment to catalyze reactions that break down organics and side reaction materials clinging to the electrode surface. A fully self-contained PlasmaTech PE200 Plasma Processing Machine operates at 100 W for 1 minute in an oxygen environment. This catalyzes reactions that remove degraded material, resulting in resistance drop and mass loss. Pristine cathodes show no mass loss under the

same conditions, confirming that oxygen removes only degraded materials. After plasma treatment, the cathodes are washed with Dimethyl Carbonate (DMC) and dried overnight at 80°C in a vacuum oven. This cleaning process removes LiPF6 electrolyte, Li salt, and other side reaction materials from the surface. Pristine cathodes show no mass loss after five minutes submerged in DMC. Surface repair follows, applying a minimal amount of slurry to fill in cracks, holes, or regions of discoloration.

The slurry types considered include MCMB (MCMB, Carbon Black, PVDF, NMP), normal NMC slurry (NMC622, Carbon Black, PVDF, NMP), and salted NMC slurry (NMC-622, Carbon Black, PVDF, NMP, and LiTFSi at 10% wt of the NMC-622). A thin-tipped paintbrush is used for optimal slurry application, and electrodes are heated overnight at 120°C in a vacuum oven. Before assembly, the pressing stage applies 1 MPa of pressure to treated electrodes for 30 minutes at room temperature. This pressure was selected based on testing pristine NMC-622 cathodes, which showed signs of damage at pressures above 1 MPa and no thickness decrease beyond 30 minutes. Figure 2 shows the typical treatment process for cathodes with surface damage.

Figure 2: Cathode treatment evolution for moderate surface damage.

The electrodes are then reassembled into new cells. Treated cathodes undergo a Relithiation step, consisting of a discharge cycle to 2.5V at 0.01C and a CV discharge until reaching 0.002 mA (minimum allowable current for our Battery Tester). This Relithiation process restores Li ions into the correct layered lattice structure. This comprehensive remanufacturing process, shown in Figure 1, is designed to reduce operational complexity and expenses while maintaining the vital crystal structure of the electrodes. By minimizing the release of dangerous chemicals and addressing safety concerns related to waste products, our approach enhances overall safety. Applicable to both anode and cathode electrodes, this novel recycling methodology not only reduces costs and enhances safety but also preserves the crucial structural features of the electrode materials, extending their usable life and effectiveness. The figure below describes the critical steps which starts with a capacity/voltage check process before proceeding to a treatment which includes plasma treatment, washing with DMC, surface repair process where the slurry is applied to fill cracks and pressing before new cells can be assembled.

Figure 3: Facile direct recovery treatment methodology.

3. RESULTS AND DISCUSSION

As explained in Section 2, the process involves several steps. Among them, we found that three processes have critical impacts on the final recycled cell performance:

plasma treatment, salt addition, re-calendaring, and drying process. In this section, we will discuss the impact of these processes on the cathode, followed by the treatment of the anode. First, plasma treatment is essential for removing degraded materials from the electrode surface. This step significantly reduces the resistance and mass loss, improving the overall efficiency of the recycled cathode. The plasma treatment operates in an oxygen environment, which catalyzes reactions to break down organic compounds and side reaction materials clinging to the electrode surface. Second, the addition of salt to the slurry plays a crucial role in enhancing the structural integrity and electrochemical performance of the cathode. Specifically, we add LiTFSi to the NMC slurry at 10% weight of the NMC-622. This step ensures that the repaired regions have improved ionic conductivity and better integration with the existing material. Third, the calendaring process is vital for ensuring a strong connection between the new slurry and the old electrode material. By applying 1 MPa of pressure to the treated electrodes for 30 minutes at room temperature, we can achieve optimal thickness and density without damaging the electrodes. This step is crucial for maintaining the mechanical stability and electrochemical performance of the recycled cells. Lastly, a simpler drying process is introduced to replace the conventional long-duration vacuum-based drying method. For the anode treatment, we follow a similar process as the cathode process. The anodes undergo initial characterization, plasma treatment, slurry application to fill any cracks or defects. The final pressing stage ensures the anodes are properly integrated before being reassembled into new cells. By optimizing these critical processes, we enhance the performance and lifespan of the recycled full cells, making our direct recycling methodology both efficient and effective. These steps can be broadly classified into binary options (plasma treatment is applied or skiped) and actual

changes to the material condition (ie the slurry type is either normal which is unsalted or salted with LiTFSi).

3.1. IMPACT OF PLASMA TREATMENT

Plasma treatment plays a pivotal role in revitalizing used electrodes, ensuring they regain their efficiency and effectiveness. This process begins by meticulously cleaning the electrode surfaces, stripping away degraded materials, organic compounds, and side reaction products that accumulate over time. By removing these contaminants, plasma treatment prepares the electrodes for subsequent treatments, enhancing their overall performance. One of the critical benefits of plasma treatment is its ability to enhance the adhesion of new materials. When fresh slurry or coatings are applied to the electrodes, the clean and modified surfaces ensure that these new materials bond effectively. This strong adhesion is crucial for maintaining the structural integrity of the electrodes, which in turn supports the optimal storage and movement of lithium ions. Moreover, plasma treatment significantly reduces the resistance of the electrodes. By eliminating surface contaminants, the electrical conductivity of the recycled cells improves, leading to better performance. This reduction in resistance is vital for the efficiency of the battery, ensuring it can deliver power reliably. Another important aspect of plasma treatment is its role in preserving the electrodes' underlying structures. The process targets only the unwanted materials on the surface, leaving the critical crystal lattice intact. This selective removal is essential for maintaining the electrochemical properties of the electrodes, which are necessary for the battery's operation. In addition to its technical benefits, plasma treatment is also environmentally friendly. Conducted in a controlled environment, the process minimizes

the release of harmful chemicals and byproducts, making it safer for both the environment and the operators involved. This aspect of plasma treatment aligns with the broader goal of sustainable and responsible battery recycling. By integrating plasma treatment into the recycling process, we ensure that the electrodes are thoroughly prepared for further processing, such as the application of new slurry and the final reassembly into new cells. This meticulous approach not only enhances the performance and lifespan of the recycled batteries but also supports a safer and more sustainable recycling methodology.

To examine the impact of plasma treatment, we compared it to simply washing the cathodes with DMC without any plasma treatment. Plasma treatment in the presence of oxygen should catalyze reactions that remove damaged material from the surface. This allows fresh slurry to be applied only to viable electrodes with the desired layered crystal structure. Since previous testing showed that pressing is critical to cell efficacy, next the importance of plasma treatment will be evaluated. Cells follow the directions laid out in Figure 3 unless specifically noted that a step was skipped to verify its importance. CP cells undergo the normal procedure which means they were pressed and underwent plasma treatment. CN cells were NOT pressed but underwent plasma treatment. While CW cells underwent pressing and WASHING but no plasma treatment.

Table 1 provides the relevant cell information before assembly. Capacity condition denotes how the cell cycled before being opened for treatment. Zero means it had no capacity and Poor means capacity was below 30% of practical capacity but not zero. Initial mass is the mass of the cathode right before slurry is applied while Final mass is the mass after the slurry has dried. Pre-Press and Post-Press thickness represents thickness before and after pressing has been applied. Thicker cathodes are expected to get compressed more

after the re-calendaring process whereas low thickness (50-60 um) cathodes are barely impacted. The ideal cells for remanufacturing are “Zero” or “Poor” capacity cells with minimal to moderate surface damage. Cells with good capacity are damaged more than they are helped by the treatment process.

Table 1: No plasma, DMC wash only treatment history for NMC-622 half cells.

Name	**Capacity Condition**	**Surface Damage**	**Mass (mg)**		**Thickness (um)**	
			Initial	Final	Before	After
CW-01	Zero	Minimal	17.5	18.85(+1.35)	70	60(-10)
CW-02	Poor	Minimal	17.35	15.1(+0.65)	60	50(-10)
CW-03	Zero	Minimal	14	16.4(+1.00)	60	50(-10)
CW-04	Poor	Minimal	15.15	15.15(+0.35)	50	50(-0)

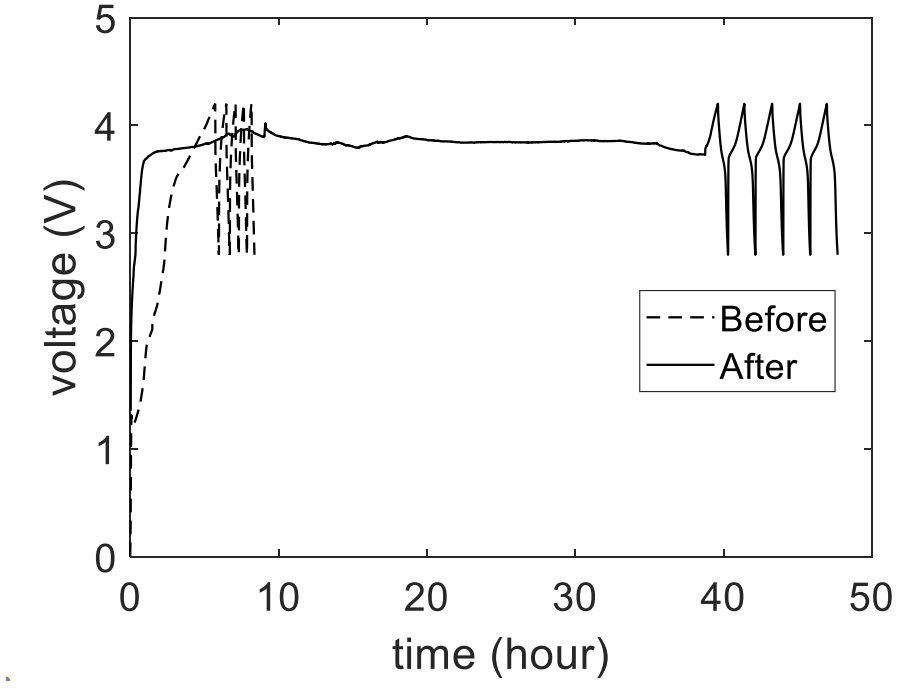

Figure 4: Voltage (top), discharging capacity & coulombic efficiency (bottom) for CW-02.

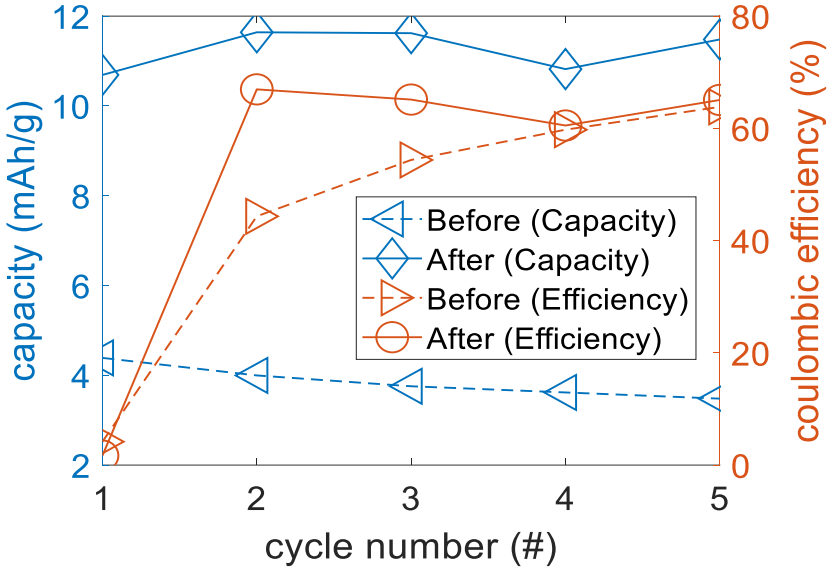

Figure 4: Voltage (top), discharging capacity & coulombic efficiency (bottom) for CW-02 (cont.).

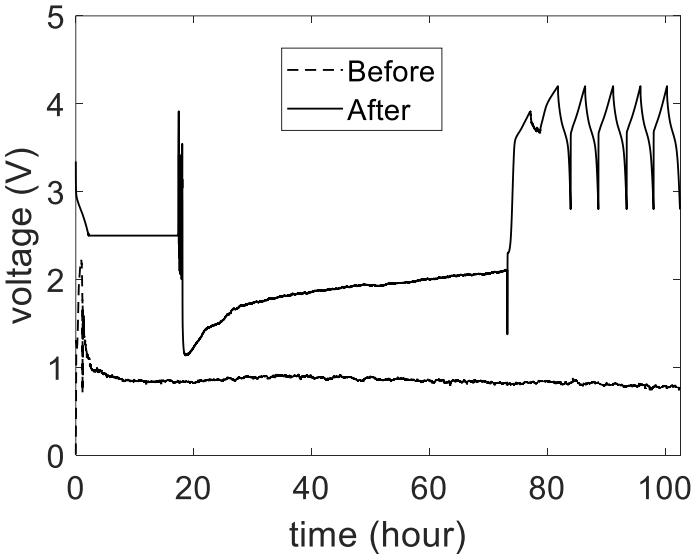

Figure 5: Voltage (top), discharging capacity & coulombic efficiency (bottom) for CW-03.

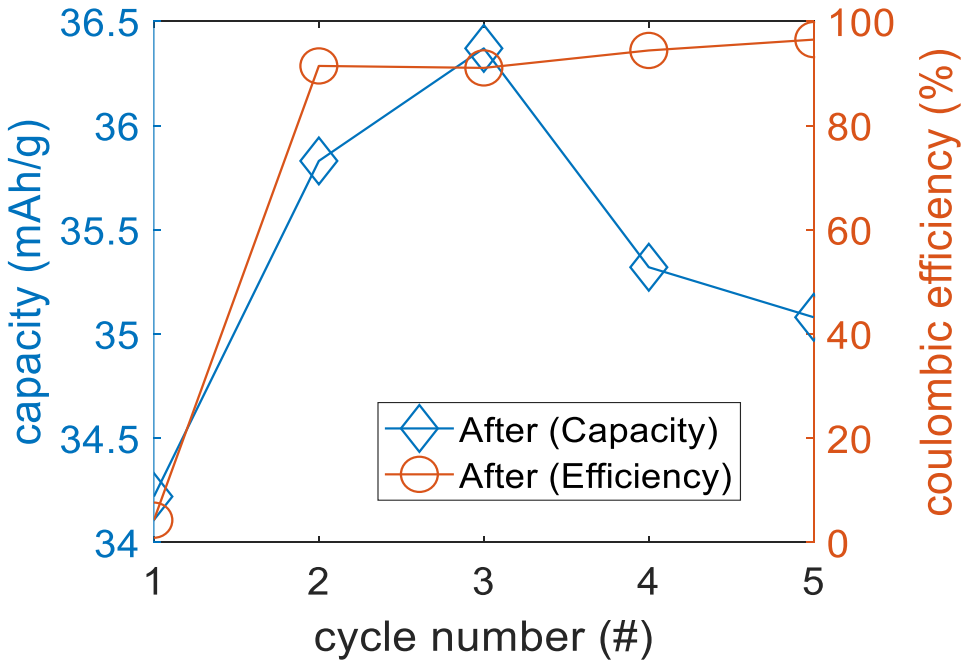

Figure 5: Voltage (top), discharging capacity & coulombic efficiency (bottom) for CW-03 (cont.).

Table 2: Capacity performance of no plasma, DMC wash only for half cells.

Name	**Before Treatment (mAh/g)**				**After Treatment (mAh/g)**				
	Ch(1^{st})	Dc(1^{st})	Ch(5^{th})	Dc(th)	ReLi	Ch(1^{st})	Dc(1^{st})	Ch(5^{th})	Dc(th)
CW-01	Zero				2.22	Zero			
CW-02	91.51	3.82	4.75	3.03	Zero	631.3	10.69	17.64	11.48
CW-03	Zero				9.84	1030.6	34.22	36.36	35.08
CW-04	80.88	3.41	5.71	3.40	58.4	22.41	6.32	9.27	7.70

*Ch: Charge, Dc: Discharge, ReLi: Relithiation

Table 1 shows a lower additional mass gain for CW cells, averaging 0.84 mg compared to 2.02 mg for the previous minimal cells. This is because washed cells do not require as much additional mass, as they do not clean the surface as thoroughly as plasma

treatment does. This reduction in mass means that the pressing stage does not significantly reduce the cathode thickness. CW-04 shows a minor performance increase after treatment on a cathode with poor pre-treatment capacity. The capacity triples, however, the coulombic efficiency remains equivalent after stabilization for both scenarios. The coulombic efficiency is far lower than expected, in the 65% range compared to above 90% after stabilization. The key distinguishing feature here is the extremely long time spent in the first charging cycle. Additionally, there is no Relithiation tail because this cell had an initial voltage far below 2.5 V. A Relithiation tail represents the CCCV discharge which reinserts Li ions into the treated cathode. It generally has two regions a drop region for CC where the current is 0.01C and a flat CV region which lasts until 0.002 mA has been reached. This minimum current is the lowest that our battery tester can apply, and no tail means that Relithiation has not occurred. Cell CW-03 shows about triple the capacity performance of CW-02, with a coulombic efficiency that is 30% higher on average, at nearly 100%. It also has a distinct Relithiation tail but still shows a long first charging step that quickly stabilizes at around 35 mAh/g. Therefore, the remanufacturing works optimally for zero voltage/capacity cathodes.

3.2. IMPACT OF SALT ADDITION

The addition of salt can play a crucial role in enhancing performance and longevity. First, salt improves ionic conductivity. When salt is incorporated into the electrode material, it dissolves in the electrolyte during battery operation, thereby forming ions that significantly improve the movement of lithium ions between the anode and cathode during both charging and discharging cycles. This enhancement in ionic conductivity is crucial as

it accelerates the rate at which lithium ions can migrate within the electrode structure, facilitating quicker and more efficient energy transfer. Moreover, salt helps stabilize the electrode structure. It fills in voids and cracks within the electrode, ensuring that the active materials remain in close contact with the conductive carbon network and current collectors. This structural integrity is vital for maintaining consistent performance throughout the battery's lifecycle. In the recycling process, salt is particularly important for re-lithiating the electrode material. Over time, cathodes can lose lithium ions, reducing their capacity and efficiency. By adding salt, lithium ions are reintroduced into the electrode, restoring much of its original performance and efficiency. In the slurry preparation process for electrode manufacturing, salt ensures a more uniform and stable mixture. This uniformity means that the active material, conductive additives, and binder are evenly distributed, leading to better electrode performance and consistency.

To assess the impact of LiTFSi salt, it was added to the slurry to enhance the Relithiation of spent cathode material. The objective was for this additional lithium to migrate into the aged material, aiming to restore its performance comparable to that of fresh slurry. Cathodes denoted as CU-## were treated with unsalted normal slurry, while CS-## cathodes were treated with salted slurry. Both CU and CS cells underwent standard treatment processes, differing only in the type of slurry used. The spent cells used in this study were sourced separately from previous tests, necessitating the comparison with cells treated using normal slurry. After treatment, CU cells were categorized based on their performance: total failure (CU-01, CU-05), slight capacity changes (CU-04, CU-06), and significant improvement (CU-02, CU-03).

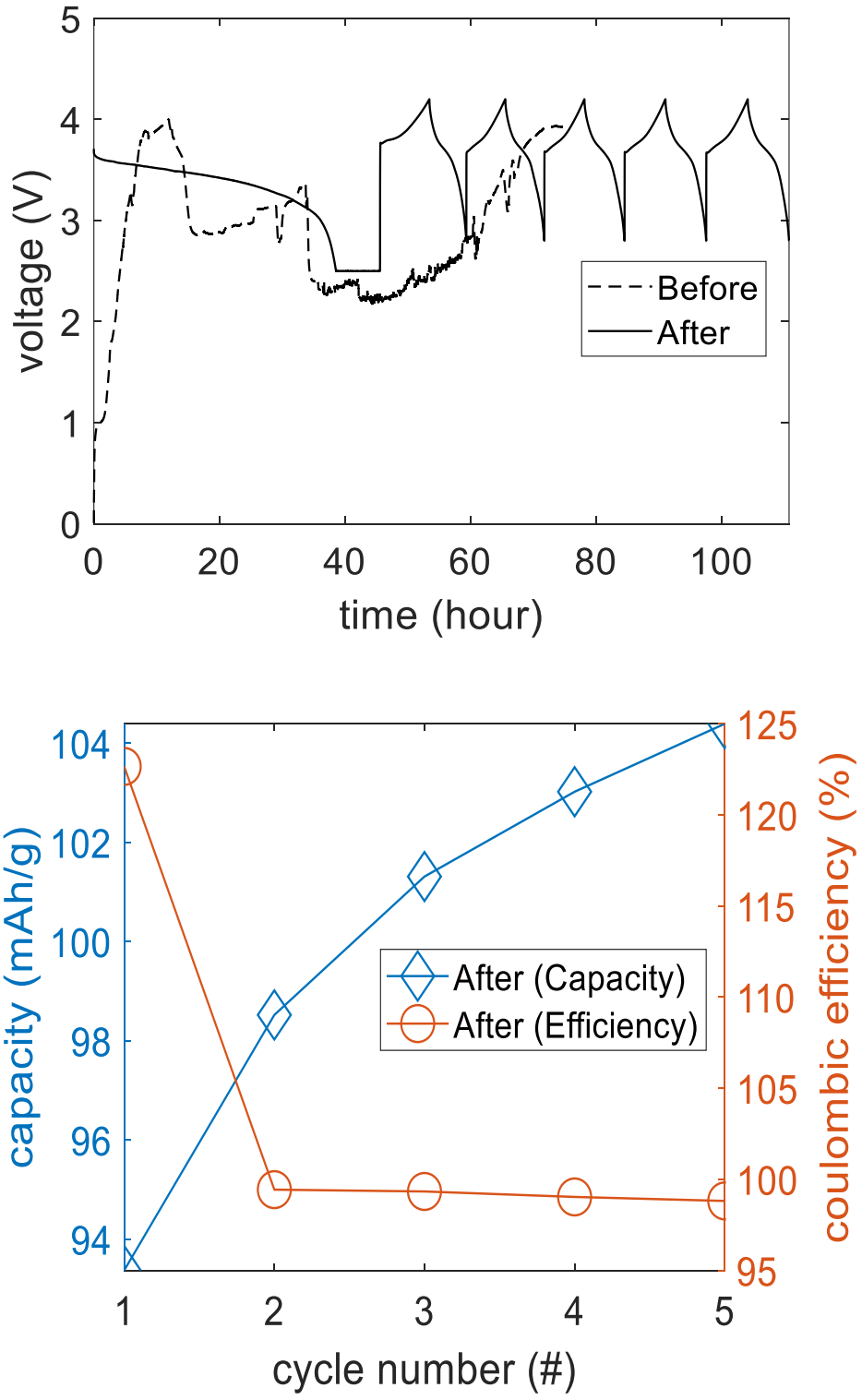

Figure 6: Voltage (top), discharging capacity & coulombic efficiency (bottom) for CU-02.

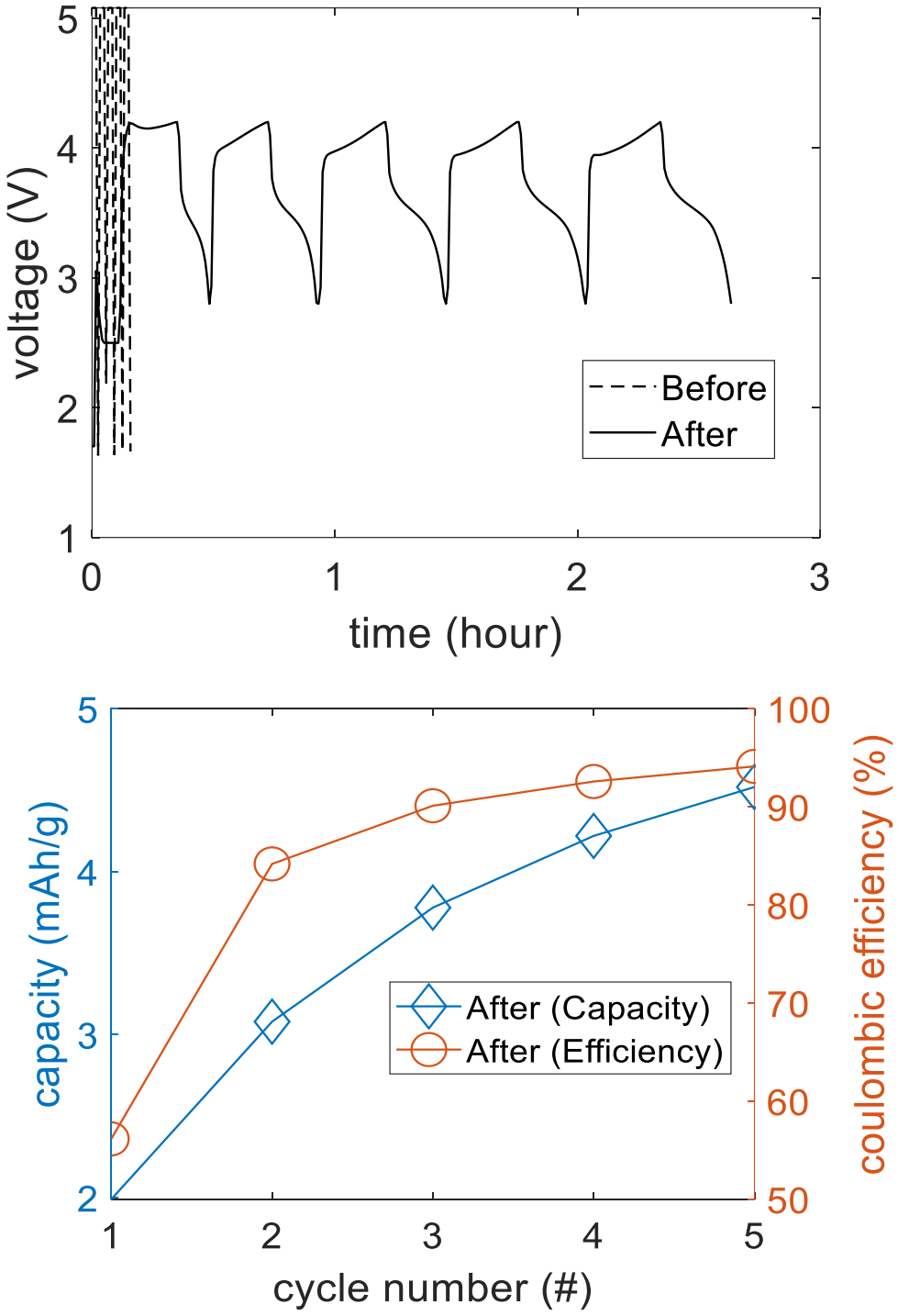

Figure 7: Voltage (top), discharging capacity & coulombic efficiency (bottom) for CS-02.

Table 3: Capacity performance of salted and unsalted for NMC-622 half cells.

Name	**Before Treatment (mAh/g)**				**After Treatment (mAh/g)**				
	Ch(1st)	Dc(1st)	Ch(5th)	Dc(th)	ReLi	Ch(1st)	Dc(1st)	Ch(5th)	Dc(th)
CU-01	103.0	5.90	5.99	4.76	Zero				
CU-02	Zero				60.5	125.4	93.97	105.6	104.4
CU-03	56.48	12.33	16.67	14.75	25.3	65.12	40.77	76.65	75.70
CU-04	Zero				92.3	26.35	8.40	12.35	10.74
CU-05	Zero				Zero				
CU-06	78.38	34.61	46.56	45.10	40.9	85.12	50.86	55.05	53.44
CS-01	Zero				Zero				
CS-02	Zero				0.07	3.67	1.99	4.81	4.52
CS-03	78.71	23.82	25.28	22.98	65.3	35.96	12.11	17.29	15.90
CS-04	98.81	88.83	88.96	88.39	9.47	0.03	0.00	0.00	0.00
CS-05	Zero				27.1	0.26	0.01	0.04	0.02
CS-06	83.85	47.38	60.38	59.29	23.5	5.90	0.00	0.01	0.00

*Ch: Charge, Dc: Discharge, ReLi: Relithiation

CS Cells demonstrate a notable decline in performance due to the addition of salt. Among these cells, only CS-02 and CS-05 showed a slight improvement after treatment, while the others either experienced a minor decrease in capacity (CS-03) or were rendered non-functional (CS-04, CS-06). Cells CS-01 exhibited zero voltage both before and after treatment. These results clearly highlight that even under the best circumstances with salted slurry, the performance is significantly inferior to that achieved with normal unsalted slurry. The primary difference lies in the much shorter Relithiation tail observed in cells treated with salted slurry, lasting only 0.05 hours compared to 7 hours for cells treated with normal slurry in this batch of spent cells. Table 3 summarizes the initial and final cycle performance before and after treatment for these cells. The highest performing salted cell,

CS-03, only achieves a capacity roughly equivalent to the lowest performing viable cell treated with unsalted slurry, CU-04. After treatment, CS-03's capacity is only 30% as good as CU-06, which is the second worst performing cell treated with unsalted slurry. Furthermore, three cells in the CS group dropped to zero or near zero capacity despite successful Relithiation, indicating poor absorption of Li ions from the salt and suggesting that the presence of LiTFSi may be forming a barrier that hinders overall performance. This issue likely stems from LiTFSi's inadequate dissolution into the slurry, thereby compromising the integration between old and new electrode materials.

3.3. IMPACT OF RE-CALENDARING

Calendaring is an essential step in battery manufacturing that focuses on shaping and enhancing the performance of battery electrodes. This process involves passing the electrode material through rollers under high pressure to compress and compact it into a thin, dense, and uniform layer. The primary goal is to improve the electrode's mechanical integrity, electrical conductivity, and overall energy storage capacity. First, calendaring helps in achieving uniform thickness across the electrode, which is critical for ensuring consistent and predictable battery performance. By compressing the electrode material, calendaring reduces the porosity and increases the packing density of active materials, conductive additives, and binders within the electrode. This densification enhances the electrical pathways and reduces internal resistance, thereby improving the efficiency of charge and discharge cycles. Moreover, calendaring improves the electrode's contact with current collectors, such as aluminum or copper foils. This intimate contact enhances the

transfer of electrons generated during charge and discharge processes, thereby improving the battery's power output and efficiency.

Additionally, calendaring helps to improve the structural stability of the electrode. It helps to align the active material particles and bind them more securely to the current collector, preventing their detachment or aggregation during battery operation. This stability is crucial for maintaining long-term performance and durability of the battery, especially under repeated cycling conditions. Furthermore, calendaring can influence the porosity of the electrode. While reducing overall porosity improves energy density and cycle life by minimizing electrolyte infiltration and enhancing electrode stability, careful control of porosity is essential. Optimal porosity allows for sufficient electrolyte penetration and accommodation of volume changes during charge-discharge cycles without compromising structural integrity.

To investigate the impact of re-calendaring in the recycling process, our experiments focus on optimizing and validating the effectiveness of this step. The calendaring process places the treated electrodes between two metal plates wrapped in Al or Cu Foil. This sandwich is then placed into the heat press where pressure is applied at 1 MPa for 30 minutes at room temperature. Applying slurry with a paint brush does not create bonds as securely or remove air pockets as effectively as a doctor blade. Pressed cathode cells (CP-##) demonstrated that 4 out of 5 cells retained discharging capacity post-treatment. In contrast, non-pressed cells (CN-##) showed discharging capacity in only 1 out of 5 cells after treatment. Table 4 summarizes the progression of pressed and non-pressed cells through the treatment process outlined in Figure 3.

Table 4: Pressing versus non-pressing treatment history for NMC-622 half cells.

Name	**Capacity Condition**	**Surface Damage**	**Mass (mg)**		**Thickness (um)**	
			Initial	Final	Before	After
CP-01	Zero	Moderate	14.1	31.1(+17.0)	170	120(-50)
CP-02	Zero	Moderate	11.8	25.1(+13.3)	150	110(-40)
CP-03	Zero	Moderate	16.7	20.3(+3.6)	100	110(+10)
CP-04	Poor	Minimal	14.3	21.3(+7.6)	150	100(-50)
CP-05	Poor	Minimal	14.7	17.0(+2.3)	120	50(-70)
CN-01	Zero	Minimal	18.5	20.0(+1.5)	NA	NA
CN-02	Zero	Minimal	16.6	19.1(+2.5)	NA	NA
CN-03	Poor	Moderate	16.1	19.7(+3.6)	NA	NA
CN-04	Poor	Moderate	15.7	18.9(+3.2)	NA	NA
CN-05	Zero	Minimal	16.5	18.4(+1.9)	NA	NA

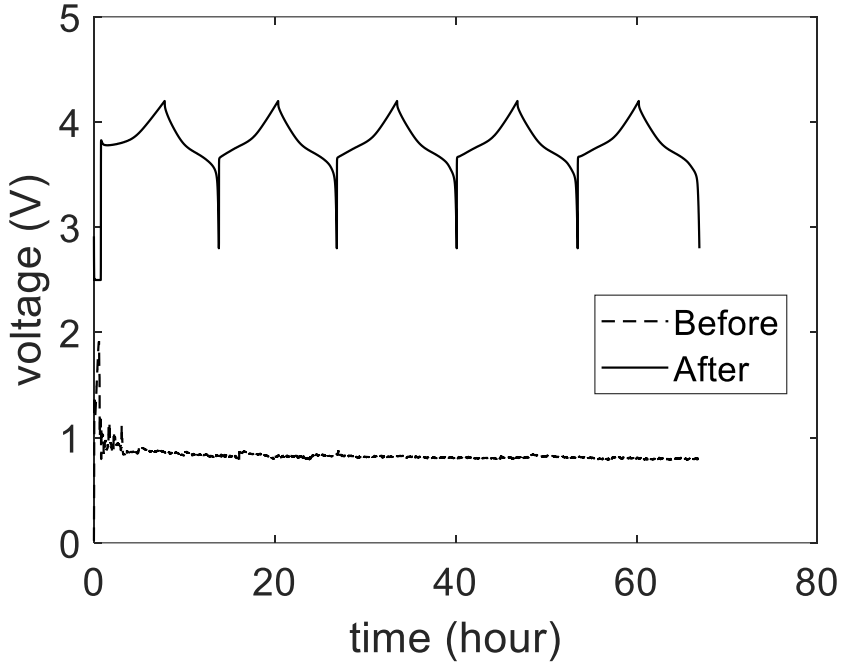

Figure 8: Voltage (top), discharging capacity & coulombic efficiency (bottom) for CP-03.

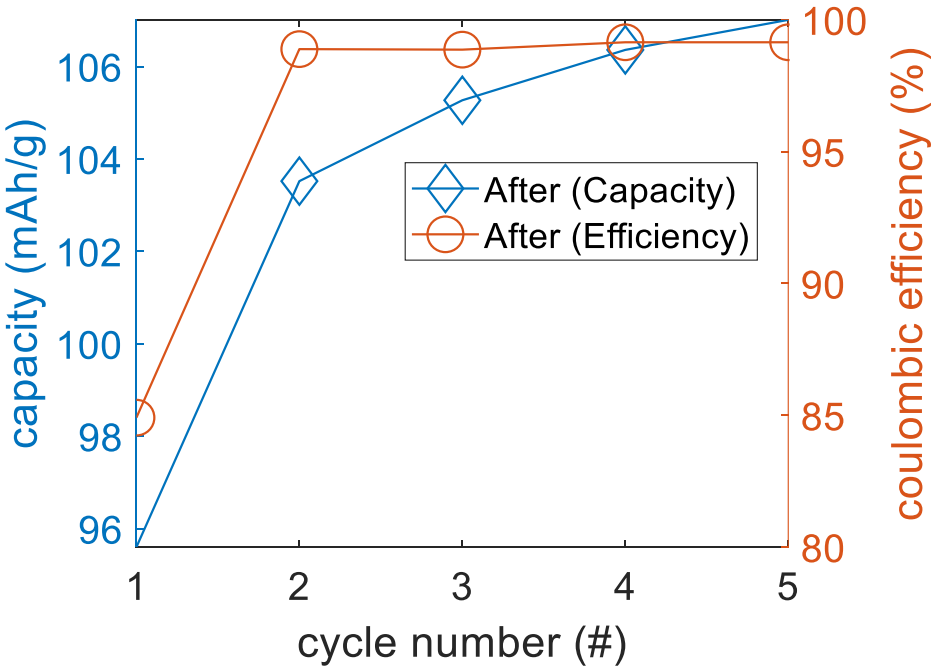

Figure 8: Voltage (top), discharging capacity & coulombic efficiency (bottom) for CP-03 (cont.).

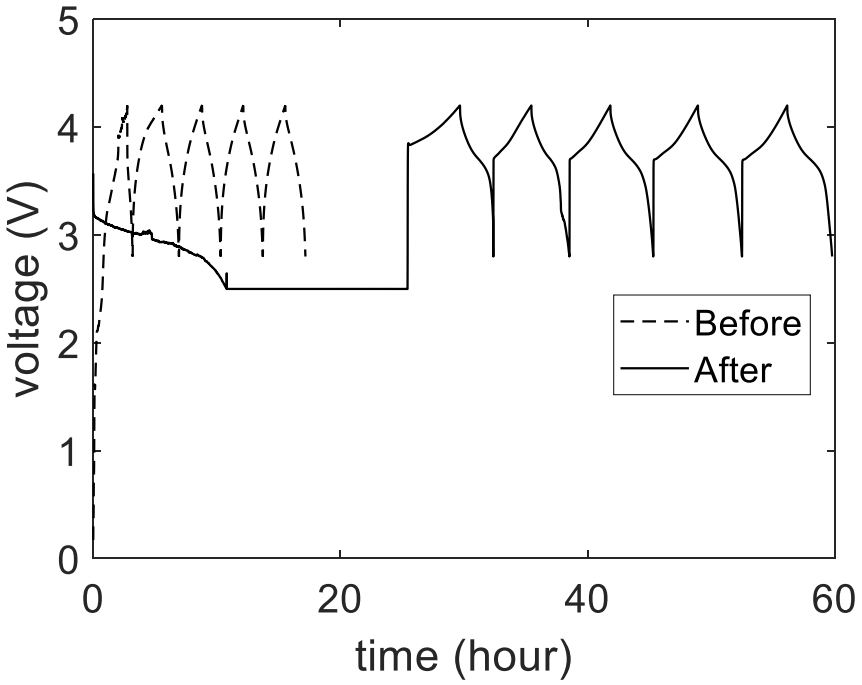

Figure 9: Voltage (top), discharging capacity & coulombic efficiency (bottom) for CP-05.

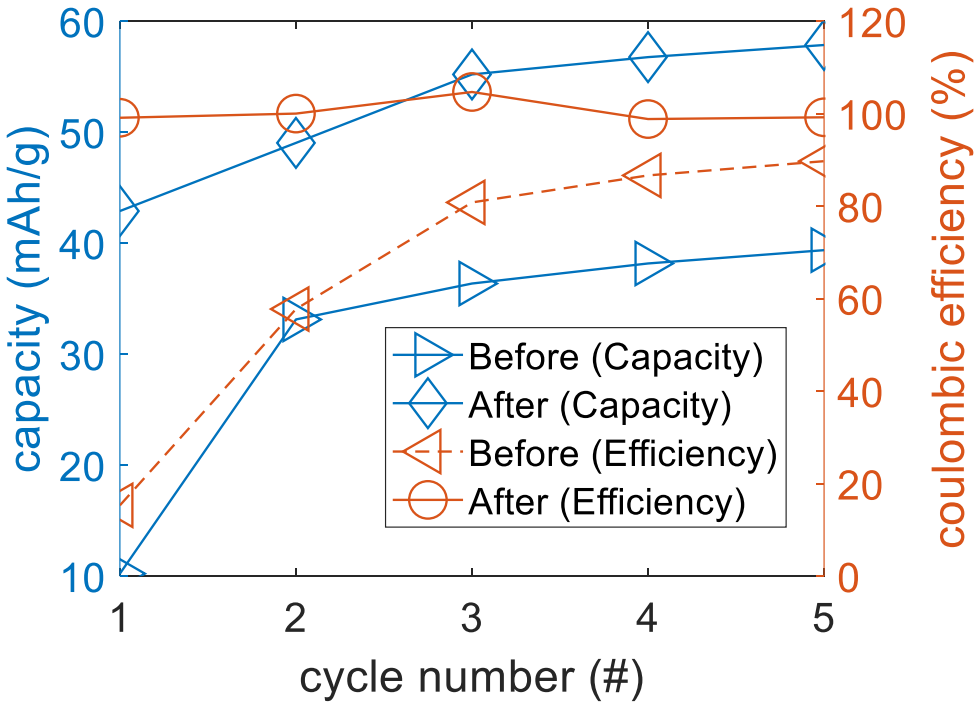

Figure 9: Voltage (top), discharging capacity & coulombic efficiency (bottom) for CP-05 (cont.).

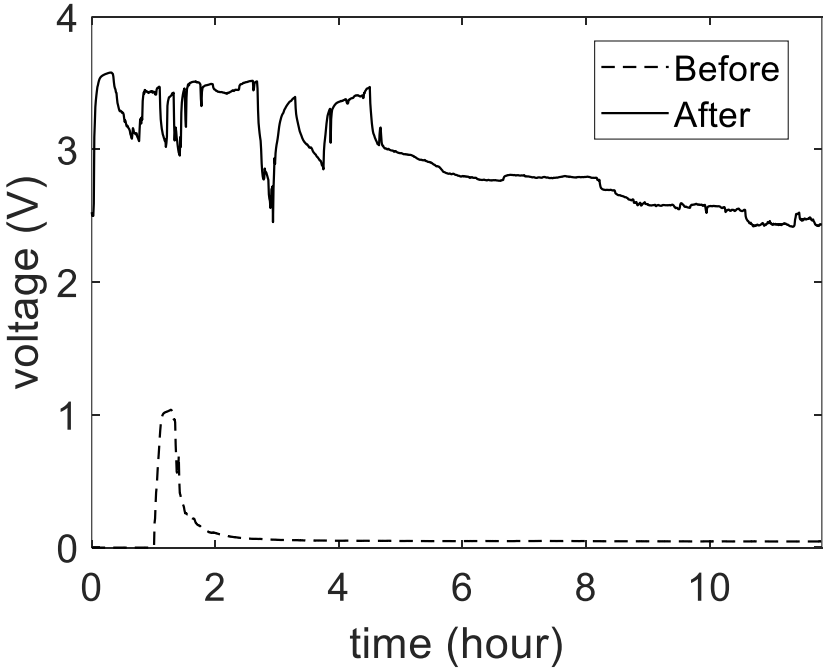

Figure 10: Voltage for CP-01.

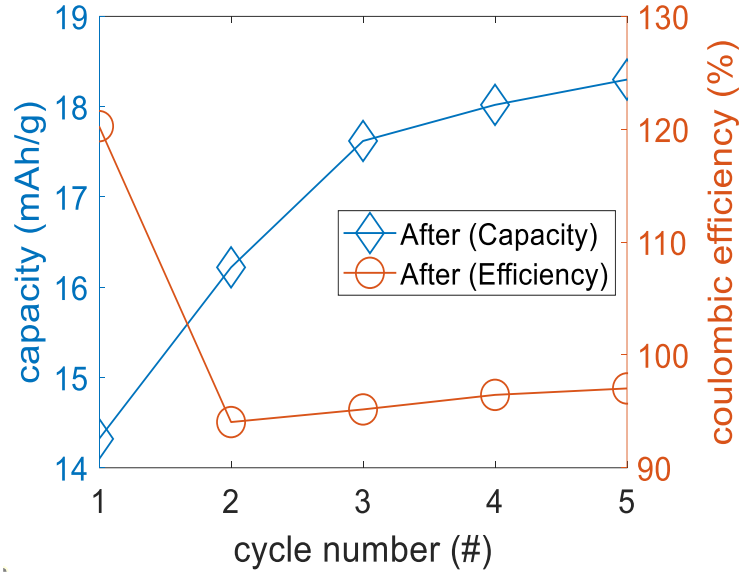

Figure 11: Discharging capacity & coulombic efficiency for CN-04.

Table 5: Capacity performance of pressed and non-pressed for NMC-622 half cells.

Name	**Before Treatment (mAh/g)**				**After Treatment (mAh/g)**				
	Ch(1^{st})	Dc(1^{st})	Ch(5^{th})	Dc(th)	ReLi	Ch(1^{st})	Dc(1^{st})	Ch(5^{th})	Dc(th)
CP-01	56.54	18.77	28.80	26.65	19.8	0.12	0.01	0.01	0.01
CP-02	Zero				0.97	105.51	89.46	99.62	98.93
CP-03	Zero				0.21	112.8	95.60	107.93	107.01
CP-04	67.27	13.49	18.77	15.55	9.79	91.39	73.29	88.59	87.54
CP-05	43.96	6.74	28.89	25.93	24.1	67.59	42.91	58.30	57.87
CN-04	Low				9.63	19.91	14.32	18.86	18.30

*Ch: Charge, Dc: Discharge, ReLi: Relithiation

The pressing stage, conducted for 30 minutes at 1 MPa, resulted in an average thickness reduction of 52.5 um for CP cells, excluding CP-03. It is worth noting that there was no thickness increase observed for CP-03; the micrometer's margin of error is 5 um. Minimal surface damage cells exhibited an average mass gain of 2.02 mg post-treatment,

while even the least damaged moderately affected cell showed a gain of over 3.00 mg. The variation in added mass among moderately damaged cells reflects the broad range of surface coverage loss in this category. The pressed cells exhibited three distinct outcomes: cells with initially zero voltage or capacity that significantly improved post-treatment (CP-02 and CP-03), cells with initial zero voltage or capacity that performed worse after treatment (CP-01), and cells with poor initial capacity that showed moderate improvement (CP-04 and CP-05).

Figures 8, 9, and 10 provide representative examples of these performance scenarios, tracking voltage behavior before and after treatment, as well as discharge and coulombic efficiency performance. In Figure 8, CP-03 initially displayed trapped voltage behavior before treatment, indicating a zero-capacity condition where voltage did not reach the 4.2 V cutoff. After treatment, the voltage behavior normalized, showing a clear Relithiation tail and stable coulombic efficiency above 99.3% by the 4th cycle. Discharge capacity increased from 90.43 mAh/g to 98.93 mAh/g over five cycles. Figure 9 illustrates CP-05, which had low initial capacity but doubled its capacity after treatment. A notable feature is the extended Relithiation tail, taking nearly a full day to complete. This suggests suboptimal integration between the old and fresh materials, even with seemingly minimal surface damage, highlighting variability in remanufacturing outcomes under apparently similar initial conditions. Contrarily, Figure 10 shows CP-01, which exhibited erratic behavior before and after treatment, without a smooth Relithiation tail. Voltage dropped to zero and did not recover, unlike CP-02 and CP-03, despite similar moderate surface damage pre-treatment. Figure 11 depicts CN-04, the only non-pressed cell with viability, albeit with low discharge capacity but high coulombic efficiency around 97%. The high

efficiency and low capacity indicate limited pathways between the cathode and current collector.

Table 5 indicates that CN-04's capacity is significantly lower compared to cells with similarly low initial capacities, such as CP-04, despite comparable coulombic efficiency post-treatment. These results underscore the critical role of pressing in post-treatment performance, as all pressed cells demonstrated capacity improvement, whereas only one non-pressed cell showed any efficacy post-treatment. Pressing ensures a robust bond between the old cathode, fresh slurry, and current collector, essential for enhancing overall cell performance.

3.4. IMPACT OF DRYING METHOD

Electrode drying is pivotal and multifaceted, serving as a crucial step in ensuring the quality, performance, and longevity of electrode materials. This process transcends mere moisture removal, playing a fundamental role in safeguarding the intricate chemistry and structural integrity of batteries. Electrodes are meticulously prepared from advanced materials poised to power a diverse array of applications. As these electrodes undergo initial fabrication and subsequent treatments, they inevitably retain moisture and volatile substances. These remnants, if left unchecked, can compromise the electrochemical properties of the electrodes and, consequently, the overall performance of the battery. In the controlled environment of a vacuum chamber, the air is evacuated, creating a low-pressure environment devoid of atmospheric gases. This reduction in pressure accelerates the evaporation of residual moisture from the electrode materials. Simultaneously, it prevents oxidation and other unwanted chemical reactions that could degrade the

electrodes' composition and structure. The meticulous control of temperature within the vacuum chamber further enhances the effectiveness of the drying process. By carefully regulating temperature levels, manufacturers ensure that moisture is removed efficiently without subjecting the electrode materials to excessive heat, which could potentially alter their physical or chemical properties.

Beyond moisture removal, vacuum drying contributes significantly to the electrochemical performance and reliability of batteries. By eliminating moisture and volatile contaminants, the electrodes maintain optimal stability and consistency throughout their operational life. This consistency is crucial for achieving predictable and reliable battery performance across production batches. Moreover, vacuum drying plays a critical role in maintaining the dimensional stability of electrode materials. As moisture is expelled, the electrodes retain their intended shape and structure, which is essential for precise assembly into battery cells. This dimensional stability ensures uniformity in battery manufacturing processes, minimizing variations that could affect battery performance and lifespan.

This section examines whether the drying process should be repeated for recycling or if a simpler method can be introduced. In this work, we introduce a simple process that involves heating hot plates under atmospheric conditions at around 70°C. This is followed by a final drying step at room temperature in a vacuum oven overnight (12-14 hours) ensuring complete dryness of the slurry to prevent tearing during the pressing process. This adjustment was driven by concerns that overnight heating at 120°C was damaging the old cathode material. Even lower temperatures, ranging from 100°C to 150°C, have been demonstrated to compromise the cohesion between electrodes and current collectors in

spent cells due to the decomposition of PVDF [27]. Additionally, some literature suggests that oxygen exposure might play a crucial role in restoring the correct crystalline structure for degraded cells and so drying under atmospheric conditions accounts for this factor.

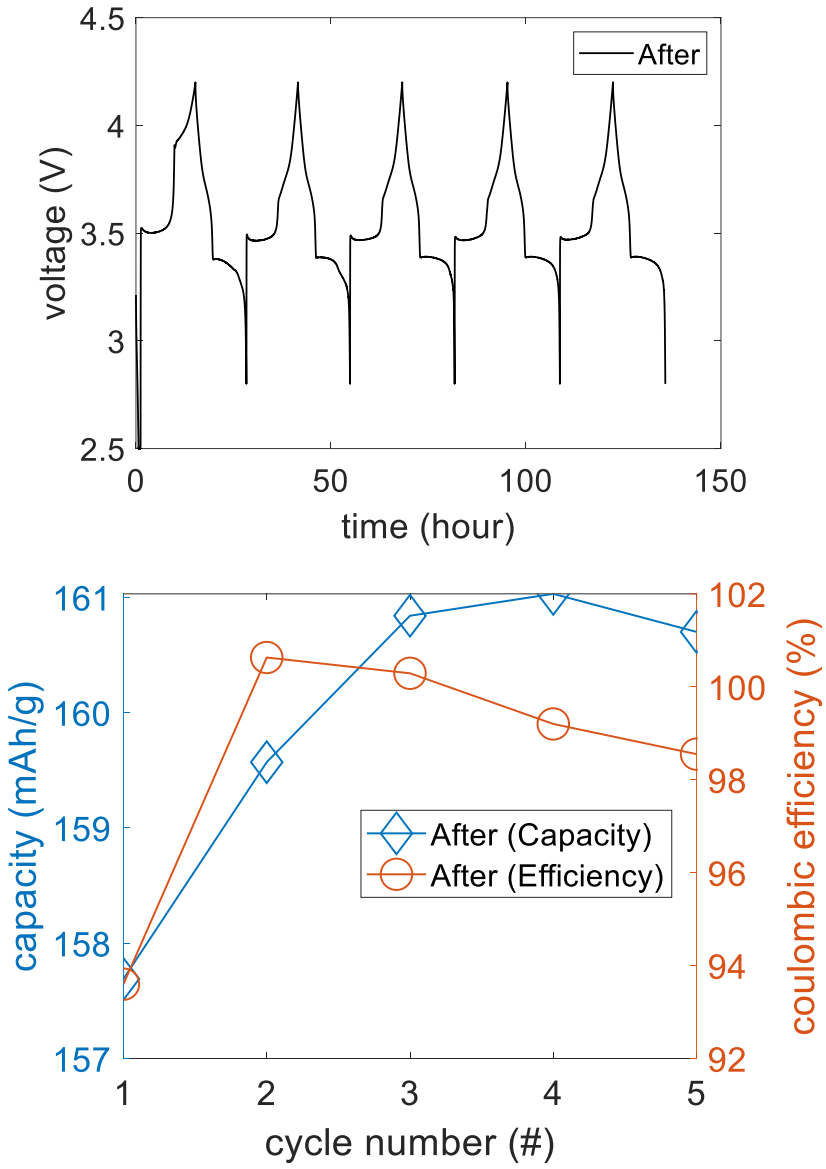

Figure 12: Voltage (top), discharging capacity & coulombic efficiency (bottom) for HP-01.

Figure 12 illustrates the initial test case of a ‘Zero’ voltage/capacity cathode with ‘Minimal’ surface damage. This new methodology demonstrates complete restoration of performance, achieving a practical capacity of 160 mAh/g for NMC-622 when using Li-Foil Anodes. To further evaluate this process, cathodes were bisected and subjected to two drying methods: the standard slurry drying process at 120°C for 12-14 hours (overnight) and drying on a hot plate at 67°C for 1 hour followed by room temperature drying in a Vacuum Oven. Cathodes were selected based on zero voltage and minimal surface damage criteria. After treatment, they were assembled into half cells with Li foil anodes. This methodology was chosen due to concerns that high temperature drying might damage the slurry. VO-## denotes the side treated with the standard vacuum oven method, while HP-## denotes the side treated with the new process. The bisection of minimally damaged cells with zero condition should allow for a direct comparison between the two treatment methodologies. This should allow for the verification of HP-01 which didn’t involve any cell bisection and serves as the test case for the new hot plate drying approach at lower temperature and under atmospheric conditions. The oxygen from the environment could be critical in regeneration of the proper crystalline cell structure.

Table 6: Bisected cathode treatment history for NMC-622 half cells.

Name	**Capacity Condition**	**Surface Damage**	**Mass (mg)**		**Thickness (um)**	
			Initial	Final	Initial	Final
HP-01*	Zero	Minimal	13.5	13.6(+0.1)	120	80(-40)
HP-02	Zero	Minimal	11.7	12.3(+0.6)	150	110(-40)
HP-03	Zero	Minimal	12.6	12.6(+0.2)	150	120(-30)
HP-04	Zero	Minimal	4.9	5.9(+1.0)	70	70(-0)
VO-02	Zero	Minimal	15.6	16.7(+1.1)	170	140(-30)

Table 6: Bisected cathode treatment history for NMC-622 half cells (cont.).

VO-03	Zero	Minimal	9.3	11.6(+2.3)	140	130(-10)
VO-04	Zero	Minimal	6.2	10.7(+4.5)	140	140(-0)

*HP-01 not bisected

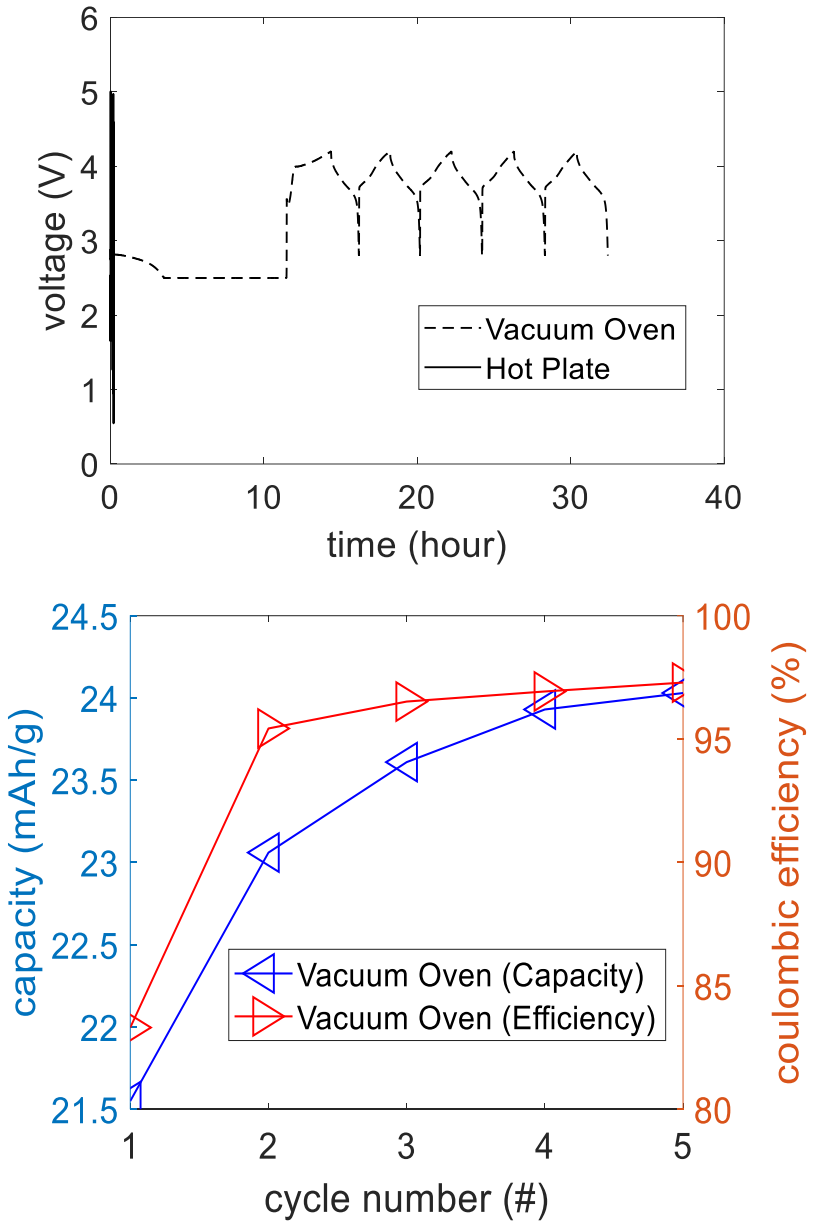

Figure 13: Voltage (top), discharging capacity & coulombic efficiency (bottom) for VO-02 & HP-02 (Cell 2).

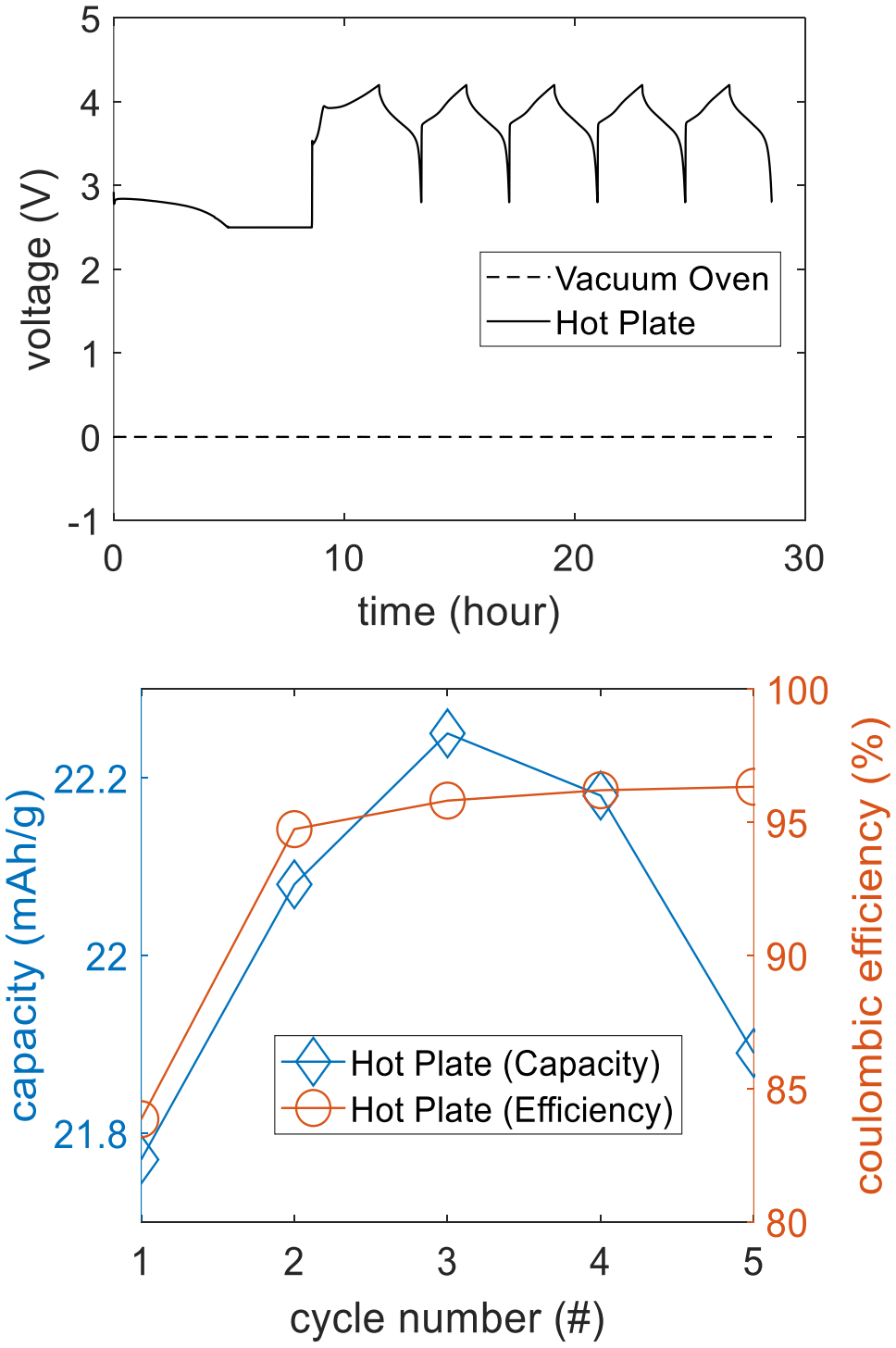

Figure 14: Voltage (top), Discharging capacity & coulombic efficiency (bottom) for VO-03 & HP-03 (Cell 3).

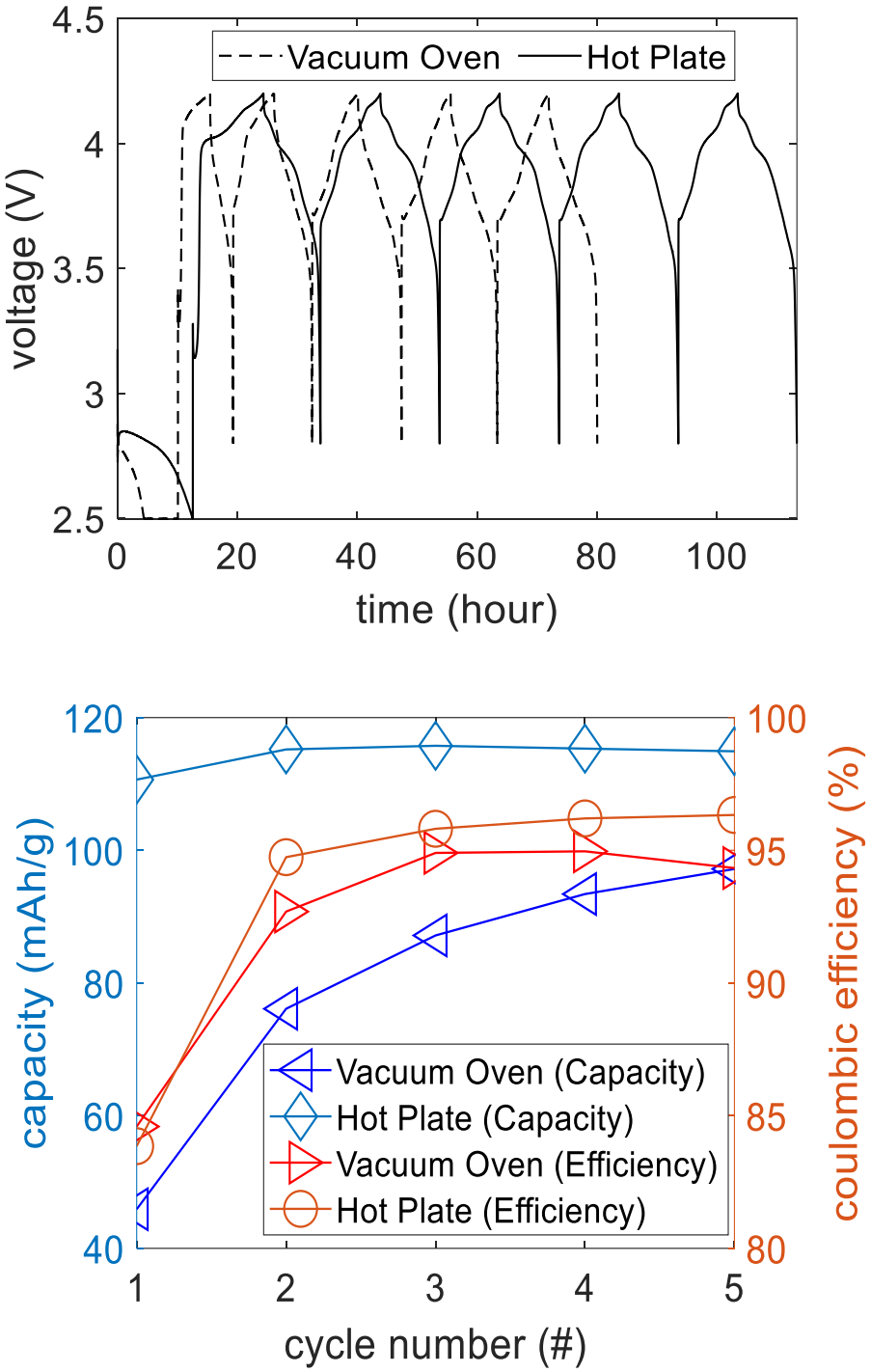

Figure 15: Voltage (top), discharging capacity & coulombic efficiency (bottom) for VO-04 & HP-04 (Cell 4).

Table 7: Capacity performance of bisected cathodes for NMC-622 half cells.

Name	**Before Treatment (mAh/g)**				**After Treatment (mAh/g)**				
	Ch(1st)	Dc(1st)	Ch(5th)	Dc(th)	ReLi	Ch(1st)	Dc(1st)	Ch(5th)	Dc(th)
HP-01	Zero				0.99	168.48	156.70	163.06	160.70
HP-02	Zero				Zero				
HP-03	Zero				7.33	34.71	21.77	22.73	21.89
HP-04	Zero				16.28	137.65	110.65	115.70	114.92
VO-02	Zero				7.99	34.99	21.55	24.70	24.03
VO-03	Zero				Zero				
VO-04	Zero				8.73	64.56	45.89	103.03	97.18

*Ch: Charge, Dc: Discharge, ReLi: Relithiation

The results show that there is not a strong correlation between the mass gained or thickness reduced in terms of cathode performance. The differences in mass can primarily be attributed to the cells not being perfectly bisected. This bisection occurs after the cathodes undergo plasma treatment, washing, and overnight drying. Cell 2 failed in the hot plate process but showed effectiveness in the vacuum oven, with an average discharge capacity of 23.66 mAh/g. Stage one of the Relithiation phase takes about 2.5 hours to drop to 2.5 V and a total of 11.49 hours. The coulombic efficiency stabilizes above 97%. Cell 3 exhibited the opposite behavior compared to Cell 2, where the hot plate method was effective but not the vacuum oven. The hot plate method had an average discharging capacity of 22.10 mAh/g. The Relithiation phase takes about 2.5 hours to drop to 2.5 V and 8.56 hours until it exits this phase. The coulombic efficiency stabilized slightly lower than VO-03, at 96%, while the discharge capacity was also marginally lower. However, no direct correlation can be drawn between HP-03 and VO-02 because these cells are unpaired

and thus we must proceed to our final cell in order to find the direct comparison that is necessary.

Cell 4 demonstrated performance for both methodologies, allowing for a direct comparison. The vacuum oven side showed an average capacity of 88.46 mAh/g, while the hot plate method reached 115.30 mAh/g. The hot plate method also achieved higher coulombic efficiency at 99%, compared to 94% for the vacuum oven. Additionally, the hot plate method demonstrated greater stability, with low cycle variance in both capacity and efficiency after the first cycle. HP-04 exhibited no Relithiation tail due to its low mass and consequently low current. However, it took longer for Relithiation at 12.42 hours compared to VO-04 at 9.91 hours. Therefore, the presence of a Relithiation tail appears to be irrelevant, with the total Relithiation time taking precedence for bisected cells.

The differences observed between the hot plate drying method and the traditional vacuum oven drying method in the performance of treated cathodes can be attributed to several critical factors, each playing a role in shaping the outcome of battery recycling processes. First, the sensitivity of electrode materials, particularly PVDF to high temperatures stands out as a primary consideration. PVDF is essential in electrode formulations for its role in binding active materials and maintaining structural integrity. High temperatures during drying in the vacuum oven may degrade PVDF, potentially compromising the cohesion between electrode components. This degradation could lead to variations in electrode thickness or composition, directly impacting battery performance metrics such as capacity and efficiency. In contrast, the hot plate drying method offers a more controlled and uniform drying environment. By heating treated cathodes at a lower temperature (around 70°C), the hot plate method aims to minimize PVDF degradation

while ensuring that the slurry dries sufficiently to prevent tearing during subsequent pressing processes. This approach not only preserves the structural integrity of the electrode but also promotes better integration between the old cathode material and the fresh slurry. The result is a stronger bond that facilitates efficient electron and ion transport during battery operation.

Moreover, the uniformity of drying across the electrode surface is crucial. The hot plate method provides more precise control over drying conditions compared to the vacuum oven, which may experience variations in drying rates and uniformity. Uniform drying is essential for ensuring consistent electrode properties and performance across different cells treated using the same method. Practical considerations such as processing time and energy efficiency also favor the hot plate method. By reducing the drying time and energy consumption compared to overnight drying in a vacuum oven, the hot plate method offers potential benefits in terms of operational efficiency and cost-effectiveness for large-scale battery recycling operations. However, despite these advantages, experimental variability and specific conditions of each method can influence outcomes. Variations in slurry composition, drying duration, and pressing parameters may introduce differences in electrode performance even when both methods aim to achieve similar treatment goals. Additionally, cell classifications such as surface damage rely upon visual determination and thus no two sets of minimally damaged electrodes are the same even if they are classified as the same. Finally, the previous history of these cells is unknown before our attempts to treat them, which also leads to variance taking place which cannot be accounted for.

3.5. ANODE TREATMENT

The treatment method illustrated in Figure 3 is also applicable to treated anode cells. The difference lies in the absence of a Relithiation step for these cells, which are assembled into full cells using fresh NMC-622 instead of Li foil. Anode treatment is not typically attempted in literature as graphene anodes are not valuable materials that are worth recovering compared to metals like Li, Co, Ni, Fe, etc. Additionally, the treatment method was created with NMC-622 as the focus so switching to MCMB anodes will require further optimization. However, showing the viability of the process on the Anode will illustrate robustness in handling electrodes with different chemical compositions which is vital for a facile process. All selected anodes exhibited 'Zero' voltage/capacity before treatment. The results are categorized into three groups: three cells failed completely, two cells (A1-01 and A1-03) showed moderate improvement, and one cell (A1-06) exhibited minimal improvement. Therefore, graphs will only be presented for cells that demonstrated improvement during the treatment process. Table 8 summarizes the general conditions of the batteries throughout the treatment process.

Table 8: Anode treatment history for MCMB full cells.

Name	**Capacity Condition**	**Surface Damage**	**Mass (mg)**		**Thickness (um)**	
			Initial	Final	Before	After
A1-01	Zero	Minimal	24.6	26.1(+1.5)	200	140(-60)
A1-02	Zero	Minimal	21.8	24.2(+2.4)	230	80(-150)
A1-03	Zero	Minimal	28.9	32.3(+3.4)	130	120(-10)
A1-04	Zero	Moderate	35.4	36.0(+0.6)	70	70(-0)
A1-05	Zero	Moderate	25.1	30.8(+5.7)	230	180(-50)
A1-06	Zero	Moderate	23.0	27.7(+4.7)	140	90(-50)

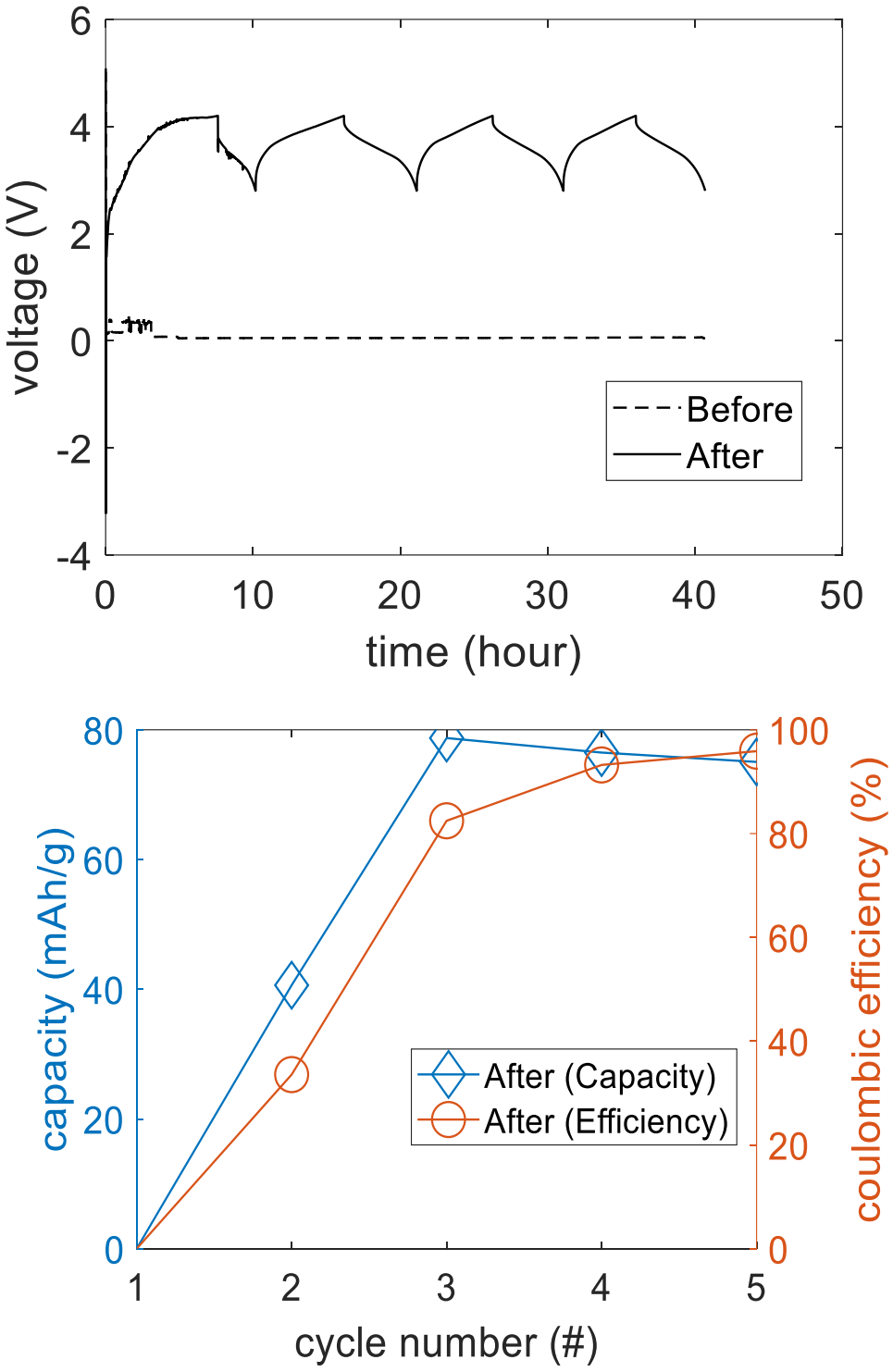

Figure 16: Voltage (top), discharging capacity & coulombic efficiency (bottom) for A1-01.

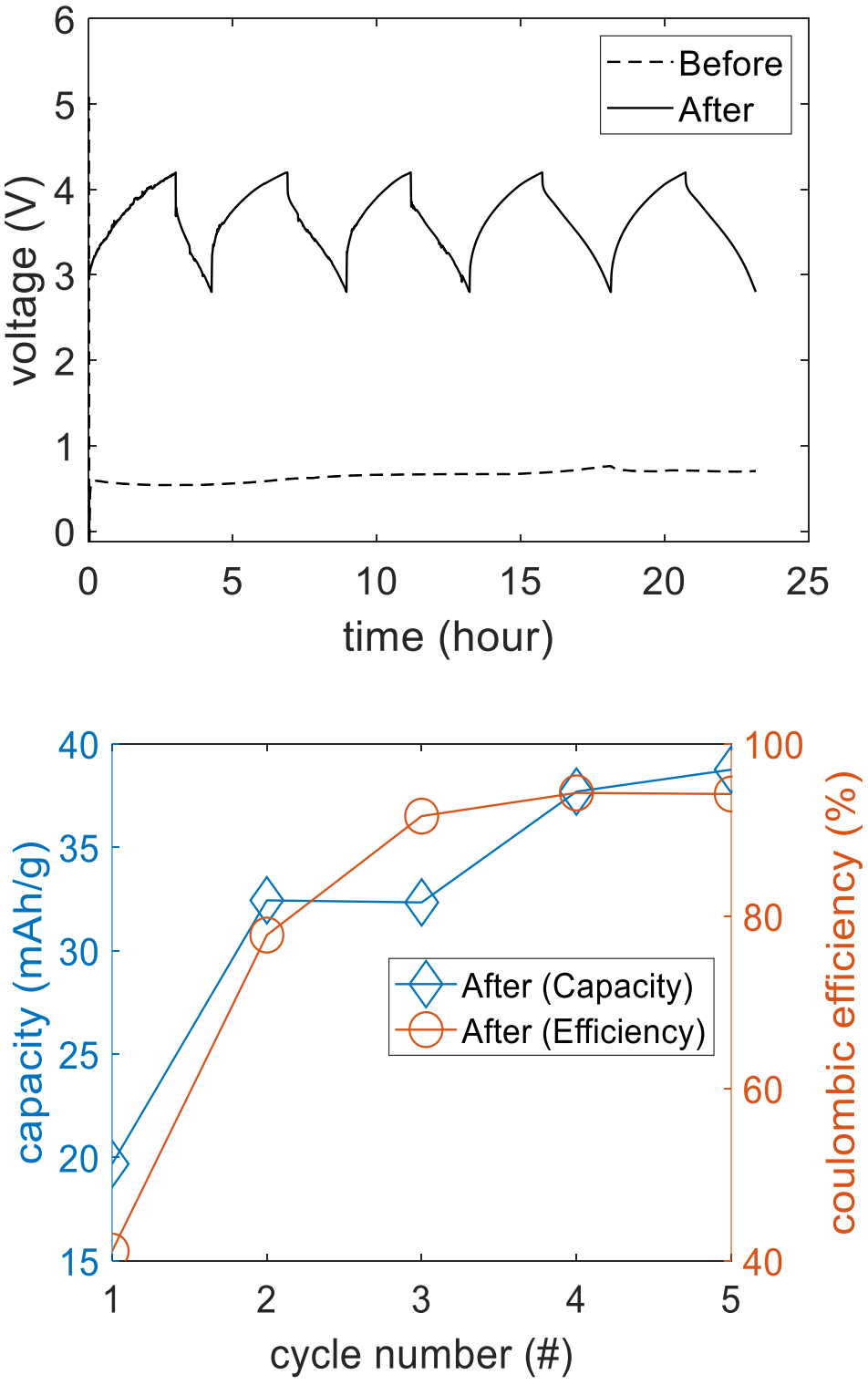

Figure 17: Voltage (top), discharging capacity & coulombic efficiency (bottom) for A1-03.

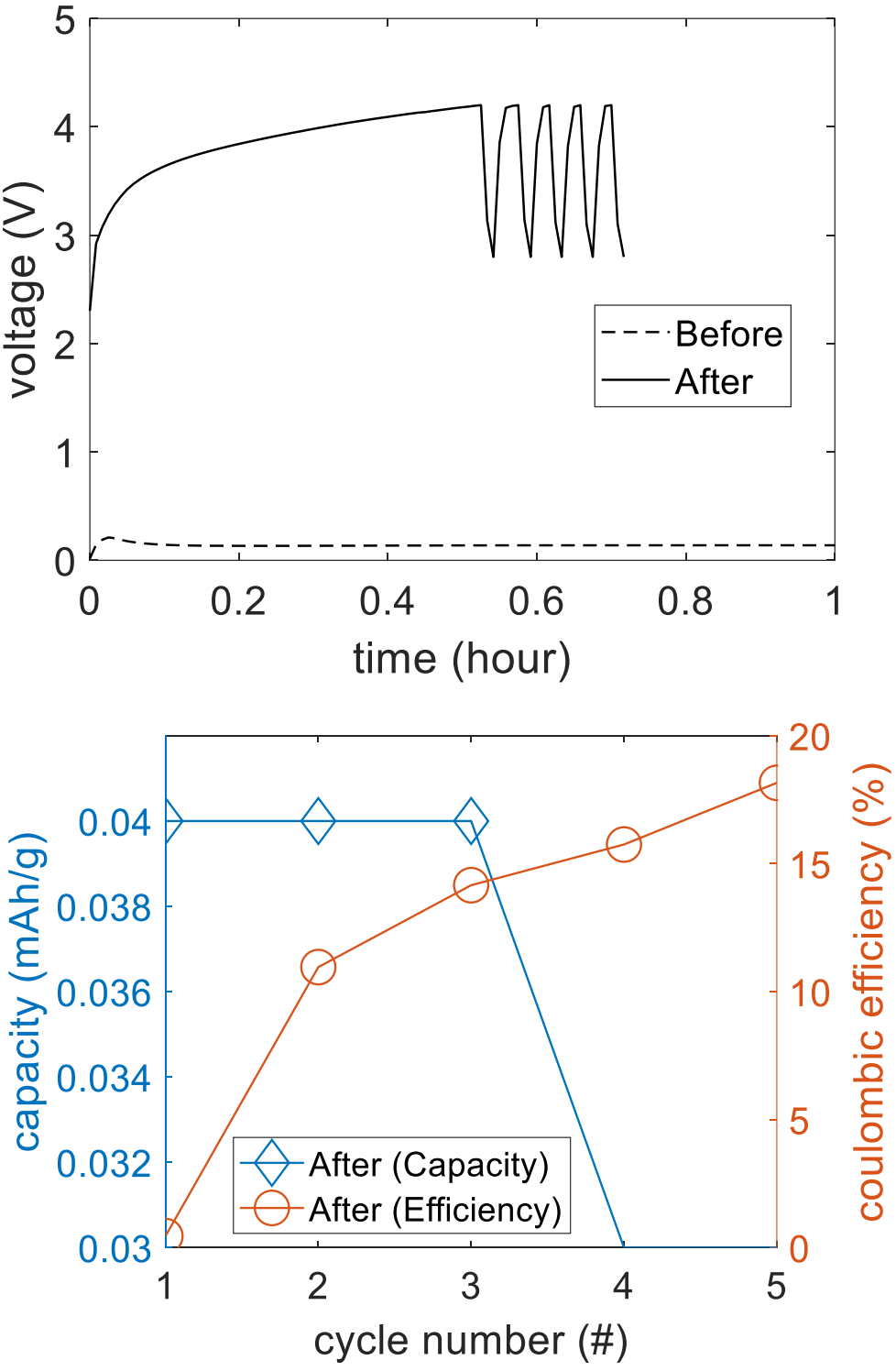

Figure 18: Voltage (top), discharging capacity & coulombic efficiency (bottom) for A1-06.

Table 9: Capacity performance of anodes for MCMB full cells.

Name	**Before Treatment (mAh/g)**				**After Treatment (mAh/g)**				
	Ch(1^{st})	Dc(1^{st})	Ch(5^{th})	Dc(th)	ReLi	Ch(1^{st})	Dc(1^{st})	Ch(5^{th})	Dc(th)
A1-01	Zero				NA	0.00	0.00	78.28	75.04
A1-03	Zero				NA	47.9	19.89	41.44	38.75
A1-06	Zero				NA	8.31	0.04	0.17	0.03

*Ch: Charge, Dc: Discharge, ReLi: Relithiation

Table 8 displays significant variability in anode thickness before and after pressing, which appears unrelated to the added mass or changes in thickness. However, both minimally damaged cells show similar final thicknesses: A1-01 at 140 um and A1-03 at 120 um. In Figure 16, the first discharge cycle exhibits irregular behavior, which affects subsequent cycles. By the third cycle, stability is achieved with a high capacity close to 80 mAh/g and nearly 100% coulombic efficiency. A1-03 performs approximately half as well as A1-01, reaching only 40 mAh/g in capacity, with efficiency stabilizing around 95%. A1-06 shows poor performance in both capacity and efficiency, suggesting that the treatment process is most effective for cells with minimal surface damage, consistent with the results seen in cathodes.

Table 9 illustrates that MCMB anodes take longer to stabilize their discharge capacity compared to cathodes undergoing the standard remanufacturing process. A1-01 starts from an initial value of 0.00 before rising to a respectable 75.04 mAh/g, while A1-03 doubles over five cycles. However, these values are well below the near 100 mAh/g or higher capacities achieved by the best cathode cells. Therefore, further optimization may be necessary, not only for moderately damaged cells but across the board.

3.6. FUSING TREATED ANODES AND CATHODES

Since the treatment method introduced in Figure 3 has shown to be viable for both cathodes and anodes, the final stage is trying to fuse two treated electrodes into single working full cell. This is not typically attempted in literature as treated electrodes are almost always assembled into cells with a fresh electrode or Li foil. All selected electrodes exhibited 'Zero' voltage/capacity before treatment and there was no Relithiation step for cathodes. FA-## means Fusion Anode while FC-## means Fusion Cathode and the numbers after representing the pair. Table 10 summarizes the treatment evolution for these treated pairs. Lower capacity is expected because a one step process is attempted where cathodes do not undergo the typical re-lithiation.

Table 10: Cathode and anode treatment history of fusion cells for full cells.

Name	**Capacity Condition**	**Surface Damage**	**Mass (mg)**		**Thickness (um)**	
			Initial	Final	Before	After
FA-01	Zero	Minimal	24.9	29.0(+4.1)	100	60(-40)
FA-02	Zero	Minimal	22.8	26.7(+3.9)	120	60(-60)
FA-03	Zero	Minimal	32.0	32.4(+0.4)	80	40(-40)
FA-04	Zero	Minimal	27.6	33.7(+6.1)	150	80(-30)
FC-01	Zero	Minimal	20.2	20.3(+0.1)	60	30(-30)
FC-02	Zero	Minimal	29.8	26.7(+3.9)	180	120(-60)
FC-03	Zero	Minimal	24.2	28.5(+4.3)	160	100(-60)
FC-04	Zero	Minimal	23.2	28.9(+5.7)	110	80(-30)

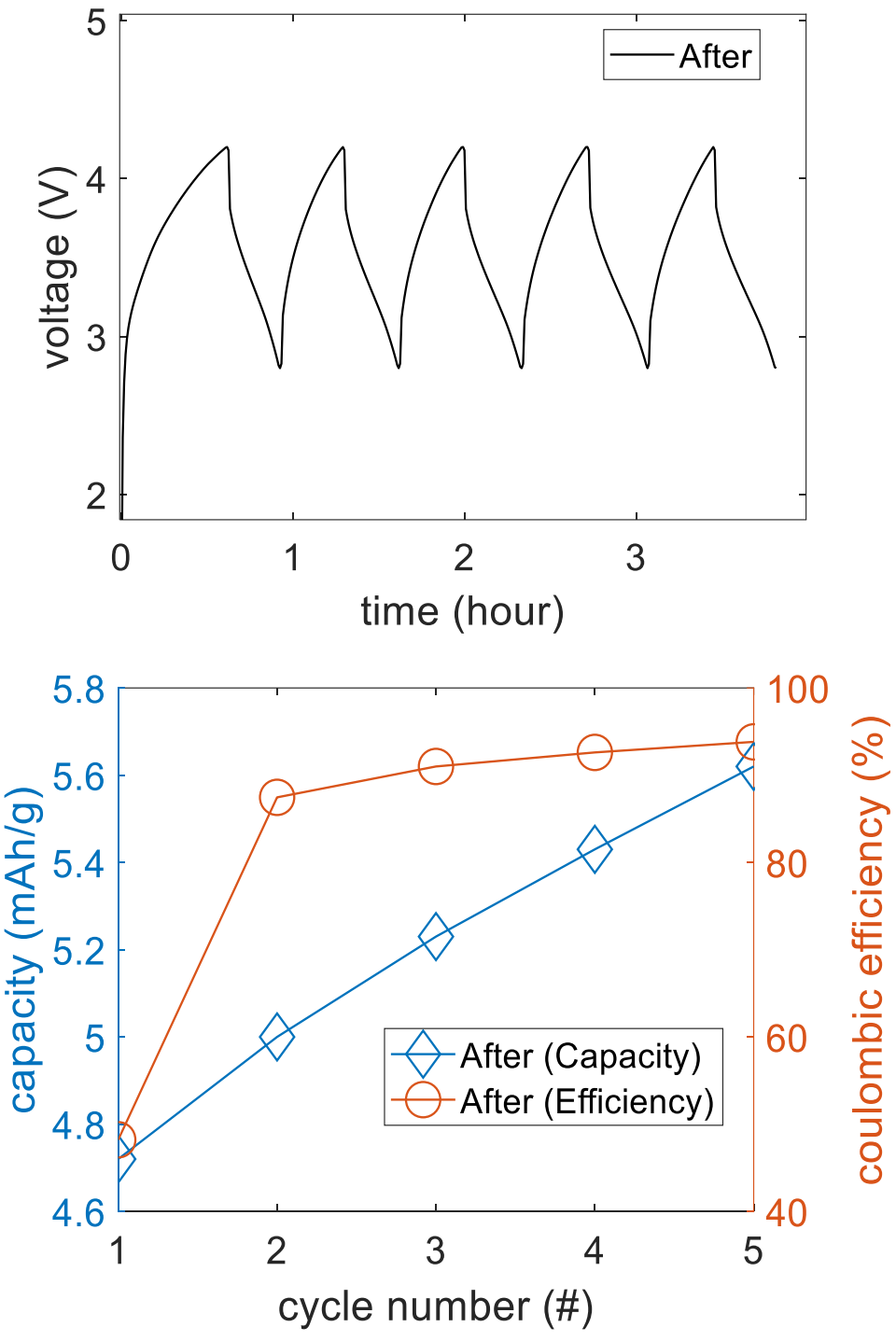

Figure 19: Voltage (top), discharging capacity & coulombic efficiency (bottom) for FA-01 & FC-01 Fusion.

Despite using minimally damaged cells that are all “Zero” voltage/capacity condition, the results for fusion are very poor. Only one cell fusion (FA-01 & FC-01) is viable with a low capacity of 5.20 mAh/g and a coulombic efficiency that stabilized at 92%. This poor performance suggests that cathodes might require Relithiation with Li foil before full cells can be assembled. However, this would require multiple openings of cells which introduces more opportunities for surface damage to occur. Additionally, the cathode would have to be removed inside the glove box to limit any environmental interactions. Thus, it is favorable to attempt to optimize a one step process before attempting a multistep process for cathodes as repeatedly opening a cell for treatment introduces more variables.

4. CONCLUSIONS

This paper shows a facile manufacturing process that while tested primarily on NMC-622 cathodes and MCMB anodes should be applicable to other common electrode chemistries. The process is optimal for highly degraded cells that show zero voltage/capacity and minimal surface damage. However, it can be applied to electrodes with poor voltage/capacity performance and moderate surface damage. The treatment process has two major components in pressing and plasma treatment. Cathodes achieved 80% efficacy with both, 50% with pressing only and 20% with plasma only post treatment. The overall efficacy was lower for anodes at 50% but the process was developed primarily for NMC-622 and less anodes were tested overall. Further, optimization is needed here.

Salting was investigated as a Li source to restore lost Li to degraded cells. Unfortunately, the remanufacturing process proved unable to properly integrate the LiTFSi Salt. Performance was universally worse as Salted cells produced lower discharging capacity although the efficacy was like normal unsalted cells.

The hot plate approach seems superior to the vacuum oven method. For a single cathode split in two, its average capacity was about 30 mAh/g higher, and its coulombic efficiency was 5% higher. For a cell that was not cut, the new method produced capacity values near the practical capacity of 160 mAh/g for NMC-622. This suggests that the higher temperature of the standard approach is damaging the cathodes due to the difference in thermal expansion between the cathode and current collector. Alternatively, oxygen from the air could play a critical role in restoring proper crystallinity to treated cathodes. Finally, while fusing a treated cathode and anode is possible, the cell viability rate is poor at 25%. Additionally, the capacity performance is very poor at 2.46 mAh/g. Thus, fusion still has plenty of room for optimization. Further, investigation is needed to verify and draw conclusions from these promising results.

ADDENDUM: EXPERIMENTAL SECTION

Materials and Paste Preparation: This paper used Li half cells which consisted of a Li Foil (0.75 mm, Alfa Aesar) anode and treated $LiN_{0.6}Co_{0.2}0Mn_{0.2}O_2$ (NMC-622) cathodes. There were three types of paste prepared for the treatment process. The normal slurry mixed 85.5 wt% NMC-622 powder (Sigma Aldrich) with 6.5 wt% Carbon Black (CB, Alfa Aesar) as the conductive agent and the binding agent was 8 wt% polyvinylidene

fluoride (PVDF, Sigma-Aldrich) and lastly was dissolved in N-methyl-2-pyrrrolidone solvent (NMP, Sigma-Aldrich). The placebo slurry consisted of simply 55 wt% CB and 45 wt% PVDF dissolved again in NMP. The salted slurry added 10 wt% Lithium bis(trifluoromethane)sulfonimide (LiTFSI, Sigma Aldrich) relative to the NMC-622 to the NMC-622, CB, PVDF which was dissolved in NMP. The manufacturer was the same for placebo and salted as the normal slurry. All slurries were mixed using a Speed Mixer (Flack Teck Inc.) at 3500 rpm for 20 minutes in air under room temperature conditions. Slurry was applied to cathodes carefully with thin tip paint brushes or slow dripping with pipettes. Paint brushes were washed with Dimethyl Carbonate (DMC, Sigma Aldrich) between usage.

Cell Opening: The cells were cracked with a crimping device where the anode extracted first. The cathodes were removed by carefully cutting the separator with a doctor blade before being lifted off with tweezers.

Measurements and Images: The weight of the cathodes was measured using a mass balance. Digital calipers measured the thickness while a portable multimeter measured the resistance. All images were shot with an iPhone 7 camera (12 MP camera). All cell cycling used a Battery Testing System (BTS, Neware).

Plasma Treatment: A machine was the PE200 Plasma Processing Machine (Plasma Etch) which used either Argon or Oxygen vacuum environment at 100 W for 1 minute. Samples were held in a petri dish to prevent them from blowing away during the vacuum creation process.

Re-Calendaring: After remanufacturing and drying, treated cathodes underwent a hot-pressing processing in air at near room temperature for 30 minutes at 1 MPa. Cathodes

were placed between two aluminum plates wrapped in aluminum or copper foil before being placed on the Lamination Hot Press (MTI). This process was initially tested on fresh NMC-622 cathode which determined that pressing at 1 MPa could be maintained up to at least 1 hour without peeling the cathode material from the Al foil.

Cell Assembly: The coin cells were assembled inside an oxygen and moisture-controlled argon-filled glove box (MBRAUN). The electrolyte was 1 M LiPF6 (lithium hexafluorophosphate) in EC: DMC (ethylene carbonate: dimethyl carbonate) 1:1 mixed by our lab. The separator was a commercially available 25 μm PP/PE/PP (polypropylene/polyethylene/polypropylene) membrane (Celgard). The cell components were ordered sequentially in the order of coin cell base, treated cathode, separator, gasket, Li foil, spacer, spring and coin cell cap before being sealed.

REFERENCES

1. Makwarimba, C., et al., *Assessment of recycling methods and processes for lithium-ion batteries.* iScience, 2022. **25**(5).

2. Bunsen, T., et al., *Global EV Outlook 2019*, I.E. Agency, Editor. 2019.

3. Paranthaman, M.P., et al., *Recovery of Lithium from Geothermal Brine with Lithium−Aluminum Layered Double Hydroxide Chloride Sorbents.* Environmental Science & Technology, 2017. **51**: p. 13841-13486.

4. Wagner, T.C., *The Lithium future—resources, recycling, and the environment.* Conservation Letters, 2011. **4**(3): p. 202-206.

5. Xu, P., et al., *A Materials Perspective on Direct Recycling of Lithium-Ion Batteries: Principles, Challenges and Opportunities.* Advanced Functional Materials, 2023. **33**(14).

6. Xiong, S., J. Ji, and X. Ma, *Environmental and economic evaluation of remanufacturing lithium-ion batteries from electric vehicles.* Waste Management, 2020. **102**: p. 579-586.

7. Wu, C., et al., *Direct Regeneration of Spent Li-Ion Battery Cathodes via Chemical Relithiation Reaction.* ACS Sustainable Chemical Engineering, 2021. **9**(48): p. 16384-16393.

8. Zhang, N., *Efficient methods for recycling cathodes of spent lithium-ion batteries*, in *Materials Engineering*. 2022, University of Alberta.

9. Hu, X., E. Mousa, and G. Ye, *Recovery of Co, Ni, Mn, and Li from Li-ion batteries by smelting reduction - Part II: A pilot-scale demonstration.* Journal of Power Sources, 2021. **483**.

10. Pinegar, H. and Y.R. Smith, *Recycling of End-of-Life Lithium Ion Batteries, Part I: Commercial Processes.* Journal of Sustainable Metallurgy, 2019. **5**(3).

11. Sojka, R., Q. Pan, and L. Billmann. *Comparative study of Li-ion battery recycling processes*. in *International Conference for Battery Recycling ICBR*. 2020. Salzburg, Austria: ACCUREC Recycling GmbH.

12. Kanoh, H., et al., Selective Electroinsertion of Lithium Ions into a Pt/λ-MnO2 Electrode in the Aqueous Phase. Langmuir, 1991: p. 1841-1842.

13. Zhang, C., et al., *Preparation of a Pt thin-film modified electrode for alkaline electrocatalytic oxidation of methanol by Cu(OH)2 electrodeposition and galvanic replacement reaction.* Electrochimica Acta, 2020. **330**(10).

14. Zhang, L., Z. Xu, and Z. He, *Electrochemical Relithiation for Direct Regeneration of LiCoO2 Materials from Spent Lithium-Ion Battery Electrodes.* ACS Sustainable Chemical Engineering, 2020. **8**(31): p. 11596-11605.

15. Choi, J.U., et al., *Recent Progress and Perspective of Advanced High-Energy Co-Less Ni-Rich Cathodes for Li-Ion Batteries: Yesterday, Today, and Tomorrow*. Advanced Energy Materials, 2020. **10**(42).

16. Guathier, M., et al., *Electrode-electrolyte interface in Li-ion batteries: current understanding and new insights.* The Journal of Physical Chemistry Letters, 2015. **6**(22): p. 4653-4672.

17. Park, K., et al., *Direct Cathode Recycling of End-Of-Life Li-Ion Batteries Enabled by Redox Mediation.* ACS Sustainable Chemical Engineering, 2021. **9**(24): p. 8214-8221.

18. Park, K.-J., et al., *Degradation Mechanism of Ni-Enriched NCA Cathode for Lithium Batteries: Are Microcracks Really Critical?* ACS Energy Letters, 2019. **4**(6): p. 1394-1400.

19. Yu, J., et al., *A redox targeting-based material recycling strategy for spent lithium ion batteries.* Energy & Environmental Science, 2019. **12**: p. 2672-2677.

20. Gao, H., et al., *Efficient Direct Recycling of Degraded LiMn2O4 Cathodes by One-Step Hydrothermal Relithiation.* ACS Applied Materials & Interfaces, 2020. **12**(46): p. 51546-51554.

21. Kim, K.D., et al., *Spinel LiMn2O4 nanorods as lithium ion battery cathodes.* Nano Letters, 2008. **8**(11): p. 3948-3952.

22. Liu, Z., et al., *Hydrothermal synthesis of nanostructured spinel lithium manganese oxide.* Journal of Solid State Chemistry, 2004. **177**(4-5): p. 1585-1591.

23. Wu, H.M., et al., *One-step synthesis LiMn2O4 cathode by a hydrothermal method.* Journal of Power Sources, 2006. **161**(2): p. 1260-1263.

24. Deng, B., et al., *Kinetic and Thermodynamic Characterization of Enhanced Carbon Dioxide Absorption Process with Lithium Oxide-Containing Ternary Molten Carbonate.* Environmental Science & Technology, 2016. **50**(19): p. 10588-10595.

25. Deng, B., et al., *Direct Recovery and Efficient Reutilization of Degraded Ternary Cathode Materials from Spent Lithium-Ion Batteries via a Homogeneous Thermochemical Process.* ACS Sustainable Chemical Engineering, 2020. **8**(37): p. 14022-14029.

26. Shi, Y., et al., *Ambient-Pressure Relithiation of Degraded LixNi0.5Co0.2Mn0.3O2 (0 < x < 1) via Eutectic Solutions for Direct Regeneration of Lithium-Ion Battery Cathodes.* Advanced Energy Materials, 2019. **9**(20).

27. Yin, H., et al., *Harvesting Capacitive Carbon by Carbonization of Waste Biomass in Molten Salts.* Environmental Science & Technology, 2014. **14**(48): p. 8101-8108.

SECTION

2. CONCLUSIONS AND FUTURE WORK

2.1. CONCLUSIONS

The new optimal charging algorithm, CGCV, proves that maintaining a constant lithium gradient by adjusting the current in relation to diffusivity is effective at boosting cell performance. The first test shows that High CGCV and Mid CGCV can both greatly reduce total charging time by 44% and 39% relative to 0.1 CCCV. However, their degradation reduction is only about 3% (12% vs 15%) which necessitated another test at 0.5C to generate charging times in line with High CGCV. Under the second test, capacity fade greatly increased at 0.5 CCCV exceeding both CGCV in 36 cycles, 20% in 60 cycles and finishing at 34% after 100 cycles. This proves that the CGCV methodology effectively suppresses crack propagation by controlling the gradient.

The remanufacturing research shows a facile remanufacturing process that while primarily tested on NMC-622 cathodes and MCMB should be broadly applicable with parameter optimization. This treatment process is optimal for treating highly degraded cells with minimal surface damage and “Zero” voltage/capacity performance prior to treatment. Although it still shows viability on poor voltage/capacity and moderate surface damage electrodes with reduced effectiveness. The key treatment components are pressing and plasma treatment. Cathodes that underwent both had 80% efficacy but only 50% with just pressing and 20% with plasma only post treatment. Anode viability after undergoing both was only at 50%.

Salted cells which attempted to replace lost Li-ions from the degraded material produced universally worse capacity post treatment. However, this did not affect cell efficacy (salted and unsalted is similar) as the LiTFSi salt proved unable to properly migrate from the fresh slurry to the old slurry.

The hot plate drying approach seems to suggest that lower temperatures and oxygen exposure are critical to cell performance post treatment. A bisected cell produced a capacity that was 30 mAh/g higher with 5% more coulombic efficiency. While an uncut cathode performance recovered to near the practical capacity of NMC-622 at 160 mAh/g. Finally, fusion of two treated cells produced poor viability at 25% and low-capacity performance at a very poor 2.46 mAh/g.

2.2. FUTURE WORK

For Optimal charging, SEM analysis of the cathode surface to determine if crack propagation is occurring could be very important to approving the algorithm. Currently, it can only be stated that crack propagation is diminished but the extent of this limitation is unclear. Additionally, the Constant Gradient profiles could be tested relative to higher C-rates to see if the effectiveness is independent of current.

Remanufacturing requires further optimization of treatment parameters especially for anodes and fusion cells which lagged in capacity performance and viability post treatment. Further studies that tweak plasma treatment energy level/duration, pressing duration/force and drying conditions could enhance performance for anodes. Of special emphasis is determining the mechanism by which hot plate drying is superior to vacuum oven drying. Thermal expansion between the cathode and current collector or Oxygen

exposure aiding in crystal structure restoration are both possible answers. Finally, verification of its effectiveness on other cells chemistries would be of great interest. Testing on anode shows that different chemistries could require unique optimization.

BIBLIOGRAPHY

1. Makwarimba, C., et al., *Assessment of recycling methods and processes for lithium-ion batteries.* iScience, 2022. **25**(5).

2. Bunsen, T., et al., *Global EV Outlook 2019*, I.E. Agency, Editor. 2019.

3. Paranthaman, M.P., et al., *Recovery of Lithium from Geothermal Brine with Lithium−Aluminum Layered Double Hydroxide Chloride Sorbents.* Environmental Science & Technology, 2017. **51**: p. 13841-13486.

4. Wagner, T.C., *The Lithium future—resources, recycling, and the environment.* Conservation Letters, 2011. **4**(3): p. 202-206.

5. Xu, P., et al., *A Materials Perspective on Direct Recycling of Lithium-Ion Batteries: Principles, Challenges and Opportunities.* Advanced Functional Materials, 2023. **33**(14).

6. Xiong, S., J. Ji, and X. Ma, *Environmental and economic evaluation of remanufacturing lithium-ion batteries from electric vehicles.* Waste Management, 2020. **102**: p. 579-586.

7. Wu, C., et al., *Direct Regeneration of Spent Li-Ion Battery Cathodes via Chemical Relithiation Reaction.* ACS Sustainable Chemical Engineering, 2021. **9**(48): p. 16384-16393.

8. Zhang, N., *Efficient methods for recycling cathodes of spent lithium-ion batteries*, in *Materials Engineering*. 2022, University of Alberta.

9. Hu, X., E. Mousa, and G. Ye, *Recovery of Co, Ni, Mn, and Li from Li-ion batteries by smelting reduction - Part II: A pilot-scale demonstration.* Journal of Power Sources, 2021. **483**.

10. Pinegar, H. and Y.R. Smith, *Recycling of End-of-Life Lithium Ion Batteries, Part I: Commercial Processes.* Journal of Sustainable Metallurgy, 2019. **5**(3).

11. Sojka, R., Q. Pan, and L. Billmann. *Comparative study of Li-ion battery recycling processes*. in *International Conference for Battery Recycling ICBR*. 2020. Salzburg, Austria: ACCUREC Recycling GmbH.

12. Kanoh, H., et al., *Selective Electroinsertion of Lithium Ions into a Pt/λ-MnO2 Electrode in the Aqueous Phase.* Langmuir, 1991: p. 1841-1842.

13. Zhang, C., et al., *Preparation of a Pt thin-film modified electrode for alkaline electrocatalytic oxidation of methanol by Cu(OH)2 electrodeposition and galvanic replacement reaction.* Electrochimica Acta, 2020. **330**(10).

14. Zhang, L., Z. Xu, and Z. He, *Electrochemical Relithiation for Direct Regeneration of LiCoO2 Materials from Spent Lithium-Ion Battery Electrodes.* ACS Sustainable Chemical Engineering, 2020. **8**(31): p. 11596-11605.

15. Choi, J.U., et al., *Recent Progress and Perspective of Advanced High-Energy Co-Less Ni-Rich Cathodes for Li-Ion Batteries: Yesterday, Today, and Tomorrow*. Advanced Energy Materials, 2020. **10**(42).

16. Guathier, M., et al., *Electrode-electrolyte interface in Li-ion batteries: current understanding and new insights.* The Journal of Physical Chemistry Letters, 2015. **6**(22): p. 4653-4672.

17. Park, K., et al., *Direct Cathode Recycling of End-Of-Life Li-Ion Batteries Enabled by Redox Mediation.* ACS Sustainable Chemical Engineering, 2021. **9**(24): p. 8214-8221.

18. Park, K.-J., et al., *Degradation Mechanism of Ni-Enriched NCA Cathode for Lithium Batteries: Are Microcracks Really Critical?* ACS Energy Letters, 2019. **4**(6): p. 1394-1400.

19. Yu, J., et al., *A redox targeting-based material recycling strategy for spent lithium ion batteries.* Energy & Environmental Science, 2019. **12**: p. 2672-2677.

20. Gao, H., et al., *Efficient Direct Recycling of Degraded LiMn2O4 Cathodes by One-Step Hydrothermal Relithiation.* ACS Applied Materials & Interfaces, 2020. **12**(46): p. 51546-51554.

21. Kim, K.D., et al., *Spinel LiMn2O4 nanorods as lithium ion battery cathodes.* Nano Letters, 2008. **8**(11): p. 3948-3952.

22. Liu, Z., et al., *Hydrothermal synthesis of nanostructured spinel lithium manganese oxide.* Journal of Solid State Chemistry, 2004. **177**(4-5): p. 1585-1591.

23. Wu, H.M., et al., *One-step synthesis LiMn2O4 cathode by a hydrothermal method.* Journal of Power Sources, 2006. **161**(2): p. 1260-1263.

24. Deng, B., et al., *Kinetic and Thermodynamic Characterization of Enhanced Carbon Dioxide Absorption Process with Lithium Oxide-Containing Ternary Molten Carbonate.* Environmental Science & Technology, 2016. **50**(19): p. 10588-10595.

25. Deng, B., et al., *Direct Recovery and Efficient Reutilization of Degraded Ternary Cathode Materials from Spent Lithium-Ion Batteries via a Homogeneous Thermochemical Process.* ACS Sustainable Chemical Engineering, 2020. **8**(37): p. 14022-14029.

26. Shi, Y., et al., *Ambient-Pressure Relithiation of Degraded LixNi0.5Co0.2Mn0.3O2 (0 < x < 1) via Eutectic Solutions for Direct Regeneration of Lithium-Ion Battery Cathodes.* Advanced Energy Materials, 2019. **9**(20).

27. Yin, H., et al., *Harvesting Capacitive Carbon by Carbonization of Waste Biomass in Molten Salts.* Environmental Science & Technology, 2014. **14**(48): p. 8101-8108.

VITA

Kasim Adesegun Adewuyi is from Greensboro, North Carolina. He earned his B.S. degree from Stanford University in Material Science and Engineering in 2014. Followed by his M.S. degree from John Hopkins University in Material Science and Engineering in 2016. Finally, he received his Ph.D. from Missouri University of Science and Technology in Mechanical Engineering in July 2024.